(2)

AD-A236 240

FINAL TECHNICAL REPORT: MODELLING OF NEARSHORE SEDIMENT TRANSPORT

Dist. A. Per telecon Mr. R. Peloquin
ONR/Code 1242

by

Daniel M. Hanes

1 March 1990 to 28 February 1991

A-1

Funded by:

The U.S. Naval Civil Engineering Laboratory

Issued by:

Department of the Navy
Office of the Chief of Naval Research
Robert A. Peloquin, Program Officer

Grant No. N00014-90-J-1619

COASTAL & OCEANOGRAPHIC ENGINEERING DEPARTMENT

University of Florida • Gainesville, Florida 32611

91-00273

91 5 21 070

DISCLAIMER NOTICE

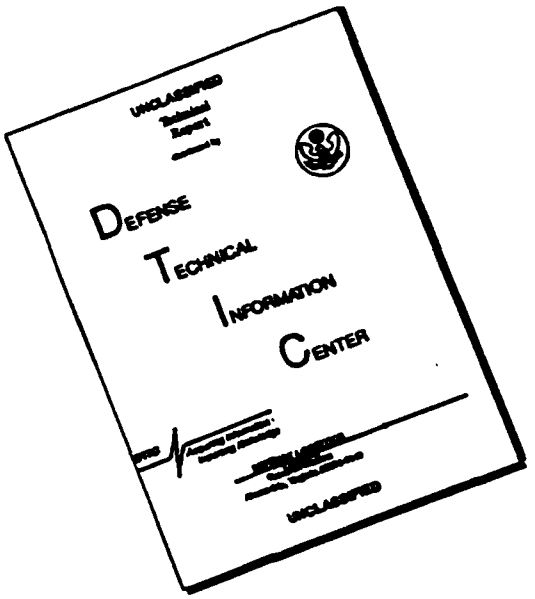

THIS DOCUMENT IS BEST QUALITY AVAILABLE. THE COPY FURNISHED TO DTIC CONTAINED A SIGNIFICANT NUMBER OF PAGES WHICH DO NOT REPRODUCE LEGIBLY.

FINAL TECHNICAL REPORT: GRANT # N00014-90-J-1619

MODELLING OF NEARSHORE SEDIMENT TRANSPORT

Project funded by:

THE U.S. NAVAL CIVIL ENGINEERING LABORATORY

Issued by:

DEPARTMENT OF THE NAVY, OFFICE OF THE CHIEF OF NAVAL RESEARCH

Robert A. Peloquin, Program Officer

Contractor:

THE UNIVERSITY OF FLORIDA

1 March 1990 to 28 February 1991

Report Submitted by:

Daniel M. Hanes, Principal Investigator
Department of Coastal and Oceanographic Engineering
University of Florida
Gainesville, Florida 32611
(904) 392-1436

Contents

Cover page	Page 1
Contents	2
Summary	3
Index of Publications	4
Appendix: Reprints of Refereed Publications	5

Summary:

This final technical report summarizes the progress achieved during the past year, which added to the work of the previous four years. Progress achieved during the first four years of the project were summarized in the Final Technical Report for Contract # N00014-86-K-0791 (to The University of Miami).

The primary effort during the past year focussed on analysis of data obtained during a field experiment conducted at Cape Canaveral during Summer, 1987. Analysis was pursued using a new approach based upon examining the spatial and temporal characteristics of individual sand suspension events, as well as their statistical characteristics. The most interesting conclusions fell along two lines of investigation: 1) the presence of wave groups enhances the suspension of sand above that which would occur with randomly distributed waves with the same height distribution; and 2) the primary difference between suspension events which cause erosion and those which cause accretion relates to the phase of the wave in which the sediment is suspended off the seabed.

Publications describing these and other findings are listed below, and refereed publications are included in the appendix.

Index of Publications, 1990-1991

Refereed Journal Articles:

1. Hanes, D. M., "The structure of events of intermittent suspension of sand due to shoaling waves", Chapter 28 in The Sea, Volume 9: Ocean Engineering Science, B. LeMehaute and D.M. Hanes (Eds), 1990, 941-952.

2. Ludwig, K., and D. M. Hanes, "A laboratory evaluation of optical suspended solids sensors exposed to sand-mud mixtures", Marine Geology, 94, 1990, 173-179.

3. Vincent, C. E., D. M. Hanes, and A. J. Bowen, "Acoustic measurements of suspended sand on the shoreface and the control of concentration by bed roughness", Marine Geology, 96, 1991, 1-18.

4. Hanes, D. M., "Suspension of sand due to wave groups", Journal of Geophysical Research, in press, 1991.

5. Dick, J.E., M.R. Erdman, and D.M. Hanes, Suspended sand concentration events due to waves over a flat seabed, in preparation.

Proceedings of Conferences and Symposia:

1. Hanes, D. M., "Geophysical Grain Flows: Report to Sponsors", Meeting Report, Transactions, American Geophysical Union, Vol. 71, No. 7, 1990, p. 274.

2. Hanes, D. M., "The intermittent suspension of sand due to shoaling waves", Euromech 262, Wallingford, England, June, 1990.

Appendix: Reprints of Refereed Publications

28. THE STRUCTURE OF EVENTS OF INTERMITTENT SUSPENSION OF SAND DUE TO SHOALING WAVES

DANIEL M. HANES

Coastal and Oceanographic Engineering Department
University of Florida

Contents

1. Introduction
2. The Stanhope Lane experiment
3. Structure of events
4. Occurrence of events
5. Cross-shore sediment transport
6. Discussion
7. Concluding remarks
Acknowledgments
References

1. Introduction

The movement of sediment by waves in coastal regions has long been considered to be a process of significance to short term bathymetric changes and to long term coastal erosion. For example, there is a prevalent seasonal trend for local storm waves to erode beaches and for swell waves to rebuild beaches. However, the detailed processes by which waves move sand are not well known, and quantitative direct measurements of moving sediment are difficult to obtain. In general, a portion of the sediment moves in suspension, with its weight supported by the action of fluid turbulence. Aspects of the transport of suspended sediment are treated elsewhere in this volume by Cacchione and Drake (Chapter 21), Kraus and Horikawa (Chapter 22), and Mehta and Dyer (Chapter 23).

Recent observations indicate that near-bed intermittent suspension is an identifiable and significant process. This chapter will describe the structure of such events observed in the field through the use of an acoustic profiling sensor. The phenomenon of intermittent suspension has been observed by several investigators including Brenninkmeyer (1976), Thornton and Morris (1978), Downing (1984), Jaffe, Sternberg, and Sallenger (1985), Sternberg, Shi, and Downing (1989), Hanes and Huntley (1986), Beach and Sternberg (1987), and Hanes et al. (1988). These observations were made at several different sites, both within and seaward of the

surf zone, and using several different instruments. A brief discussion of some of these observations within the context of intermittent suspension follows.

In the region just seaward of the wave breaking zone, Hanes and Huntley (1986) deployed a miniature optical backscatter sensor (MOBS) at Pt. Sapin, New Brunswick, and observed that both the suspension of sediment and the cross-shore transport of suspended sediment were intermittent. The suspended sediment was associated with incident waves and was enhanced during wave groups. Within the surf zone, observations of intermittent suspension have been made using fast response optical instrumentation. Using light transmission, Brenninkmeyer (1976) observed infrequent bursts of high concentrations (> 10 g/l) of suspended sediment in the surf zone and frequent bursts of extremely high concentrations (up to 500 g/l) of suspended sediment in the swash zone. Downing et al. (1985), Jaffe, Sternberg, and Sallenger (1985), and Beach and Sternberg (1987) have used optical backscatter sensors to observe intermittent suspension within the surf zone, which exhibited time scales corresponding to both incident and infragravity wave periods. Jaffe, Sternberg, and Sallenger (1985), in particular, point out the significance of intermittent suspension to cross-shore sediment transport by showing the significance of the flux coupling between fluid velocity and sediment suspension.

2. The Stanhope Lane Experiment

The experiment at Stanhope Lane, Prince Edward Island, Canada, in October, 1984 was a component of a larger study designed to examine some of the nearshore processes that occur during storms and to help understand how barred beaches respond to storms. Gillie (1985) and Daniel (1986) provide detailed descriptions of the overall C2S2 project. Descriptive observations of suspended sediment obtained with an acoustic concentration meter (ACM) have been reported in Hanes et al. (1988).

The acoustic system that was used to obtain the measurements to be described was constructed for the NOAA Atlantic Oceanographic and Meteorological Laboratories in Miami, Florida, and was first described by Huff and Fiske (1980). The primary advantages of the ACM are that it is nonintrusive and with suitable calibration can measure concentration profiles with high resolution. The initial tank calibrations were carried out by Young et al. (1982), with more detailed calibration for the C2S2 experiment described in Hanes et al. (1988). The data to be presented have temporal resolution of 0.8 sec and spatial resolution of approximately 10 percent of the distance above the sea bed for any particular measurement, but not less than 0.5 cm. The return due to the sea bed biases the concentration measurements within approximately 1.5 cm of the sea bed.

The gain of the ACM was chosen to avoid saturation at high concentrations. At the gain setting used for this experiment, the minimum resolution in concentration measurements was approximately 70 mg/l. Although this represents a high suspended sediment concentration in deeper water, the concentration at the measurement site during times of interest was on the order of 1000 to 5000 mg/l. The gain was therefore chosen to enable measurement of concentration in the 100 to 10,000 mg/l range.

The data to be discussed in this chapter were obtained at a water depth of approximately 2 m, near the crest of a longshore sand bar, designated as position

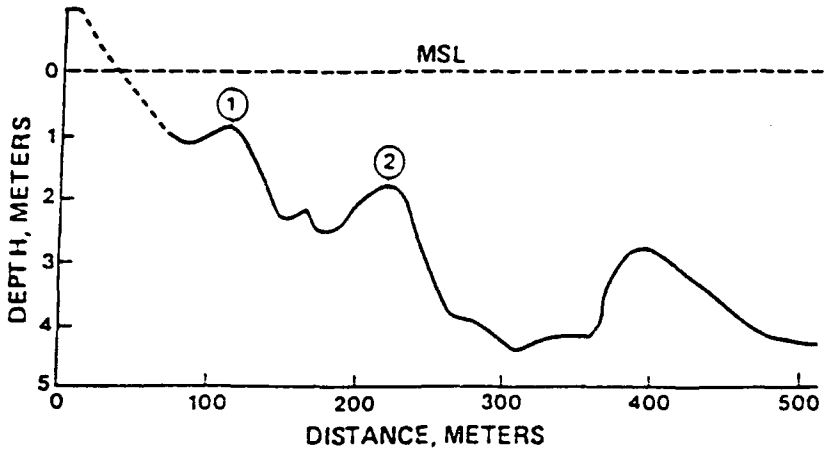

Fig. 1. Beach profile at experimental site showing location (number 2) of instrument deployment.

number 2 in Fig. 1. The sediment consisted of well sorted sand with a modal sieve size of 0.21 mm. Instrumentation consisted of an acoustic concentration meter that probed the lowest meter of the water column and an electromagnetic flowmeter located 10 cm above the sea bed. The measurements were obtained over a 410-sec period following a several day long severe storm. The tide was falling and sea level was near its mean value. The peak incident wave period was 6.1 sec, the cross-shore rms fluid speed as measured by the flowmeter was 24.0 cm/sec, and the rms wave height is estimated to have been 24 cm. We were unable to obtain accurate quantitative bed form measurements during the measurement period, but visual observations indicated ripples with lengths of order 10 cm. This data set corresponds to set D in Hanes et al. (1988).

3. Structure of Events

The time averaged suspended sediment concentration profile is given in Fig. 2. The mean concentration increases sharply in the 7-cm region near the sea bed. This is the region of interest for the remainder of this paper. The depth average of the instantaneous suspended sand concentration between the limits of 2 and 7 cm above the sea bed will be referred to in what follows as the near bottom concentration (NBC).

A time series of the NBC and fluid speed U is shown in Fig. 3, where positive U indicates that the cross-shore component of the fluid velocity is directed offshore. The suspended sediment concentration is clearly unsteady and dominated by events. The temporal structure and spatial structure of these suspension events are clarified by examining the variations in concentration on short time and space scales. We will first examine a particular event, followed by a composite description of all the events.

A particular event that occurred approximately in the middle of the record will be described. A time series of concentration at various elevations (all less than 7 cm) above the sea bed and fluid speed is shown in Fig. 4, where the elapsed time between measurements is 0.8 sec. The instantaneous concentration during the event decreases with elevation above the sea bed, as expected from the mean concentra-

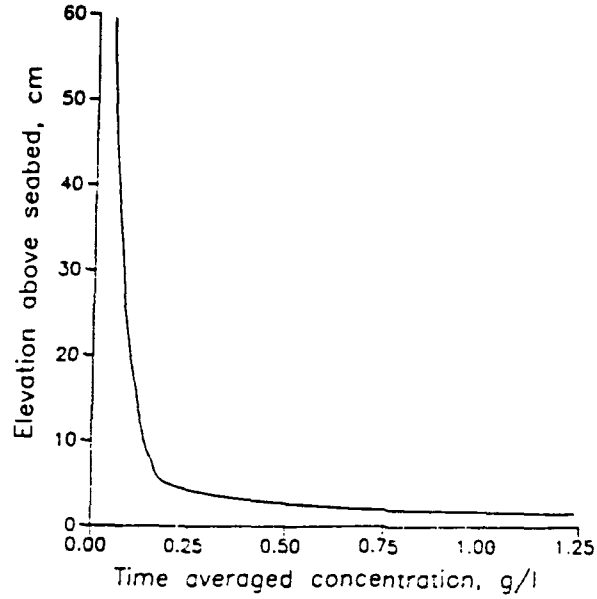

Fig. 2. The vertical profile of suspended sediment concentration averaged over 410 sec.

tion profile. This tendency is prevalent in all events. This suspension event has a time scale of approximately 3 to 4 sec and a vertical spatial scale of approximately 5 cm. For comparison, the settling velocity of the sand W_0 is approximately 2 cm/sec and U during the event averaged approximately -20 cm/sec.

A composite description of the intermittent events is obtained through a conditional sampling technique. By setting a threshold equal to the mean plus one standard deviation of the NBC for the entire record, 20 events were identified. These

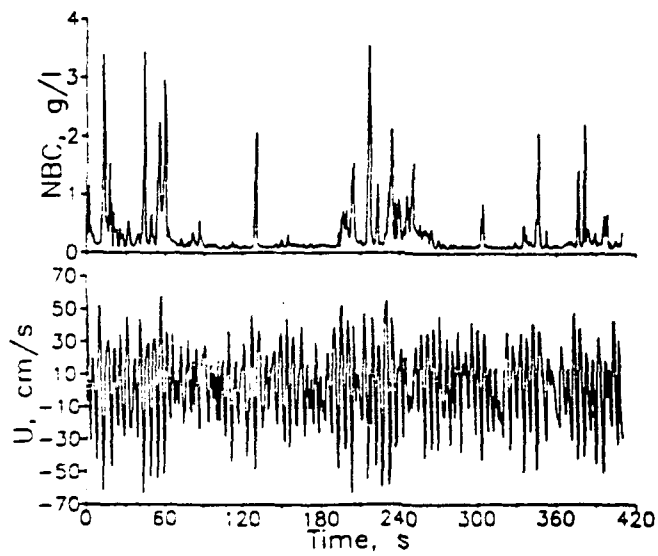

Fig. 3. Time series of depth averaged (between 2 and 7 cm above the sea bed) suspended sediment concentration (NBC) and fluid speed, where positive U indicates the cross-shore component of the fluid speed is directed offshore.

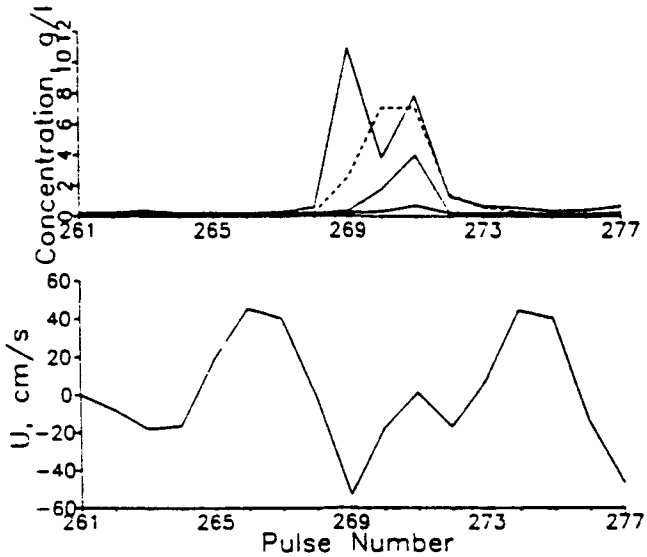

Fig. 4. Time series of suspended sediment concentration at several elevations and fluid speeds, for a particular event centered near pulse 269.

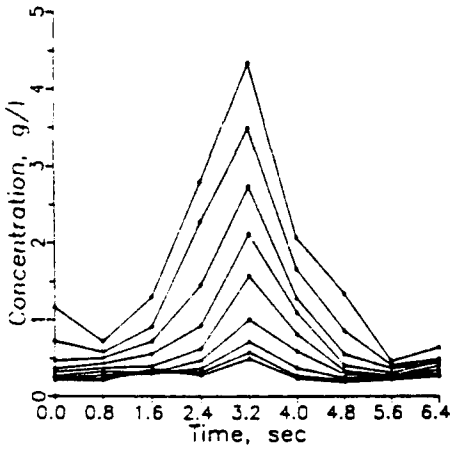

Fig. 5. Composite average for 20 suspension events of suspended sediment concentration at 2 to 6 cm elevation in $\frac{1}{2}$-cm increments. The concentration decreases monotonically with elevation, with the upper curve corresponding to 2 cm above the sea bed and the lowest curve at 6 cm above the sea bed.

20 events and the corresponding velocity measurements are then ensemble averaged by temporally aligning their maximum concentrations. The resulting average event is shown in Fig. 5. This composite event lasts for about 3 to 4 sec and has a peak concentration (at elevation 2 cm) of about 4.5 g/l. The concentration decreases sharply with distance above the sea bed, with the concentration variations negligible above about 6 cm. Also notable is the rapid increase and subsequent rapid decrease in concentration with time.

4. Occurrence of Events

The cause of the intermittency of these near bed suspension events is one of the perplexing issues that immediately arises from these observations. There are two interesting observations of relevance to this question. First, the occurrence of events is correlated with periods of higher velocity associated with groups of larger waves;

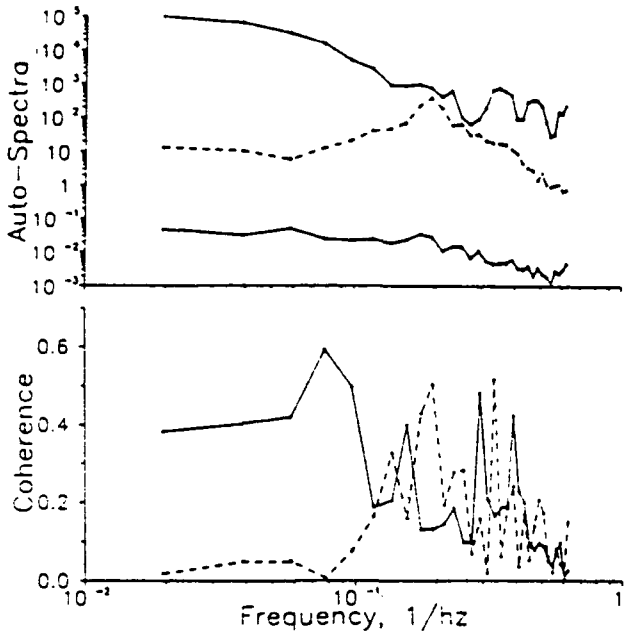

Fig. 6. Cross spectral coherence between the NBC and SKE indicates the correlation between wave groups and intermittent suspension events near periods of 30 sec. Dashed lines correspond to U, solid lines to SKE, and the lowest solid line of the upper plot is the autospectrum of NBC.

second, they initiated (in 16 out of 20 occurrences) during the shoreward phase of the cross-shore fluid motion.

From Fig. 3 it can be seen that the suspension events are usually in the midst of wave groups and rarely occur coincident with the first wave of the group. The groupiness in the velocity record is quantified by the smoothed kinetic energy (SKE), defined as $\mathrm{SKE}(t) = 1/T_p \int_{t-T_p/2}^{t+T_p/2} U^2\, dt$, where T_p is the peak incident wave period and U is the velocity time series. The correlation between the NBC and the SKE is 0.4, which is significant with above a 99 percent probability. The cross spectral coherence between the NBC and the SKE is shown in Fig. 6. Although the short duration of the overall measurement period relative to the group time scale results in large confidence intervals, the peak in coherence near a period of 30 sec is interpreted as indicative of the existence of a relationship between wave groups and suspension events (which is not yet well described).

A particularly striking example of an isolated suspension event that occurred in the middle of a wave group (at approximately 130 sec in Fig. 3) is shown with an enlarged scale in Fig. 7. This particular event is of very short duration and occurs during the shoreward phase of motion corresponding to the largest wave in the group. It is likely that there is a threshold for these events that is exceeded by either the larger waves within a group or some phenomenon associated with the sequence of larger waves.

Over the entire record length, the correlation between U and the rate of change of NBC was 0.26. Although significant, this correlation only explains a small portion of the covariations between U and NBC. The relationship between the entrainment of sediment from the sea bed and the cross-shore fluid velocity is illustrated in Fig.8, which is a scatter diagram of the rate of change of NBC verses U, for times when the

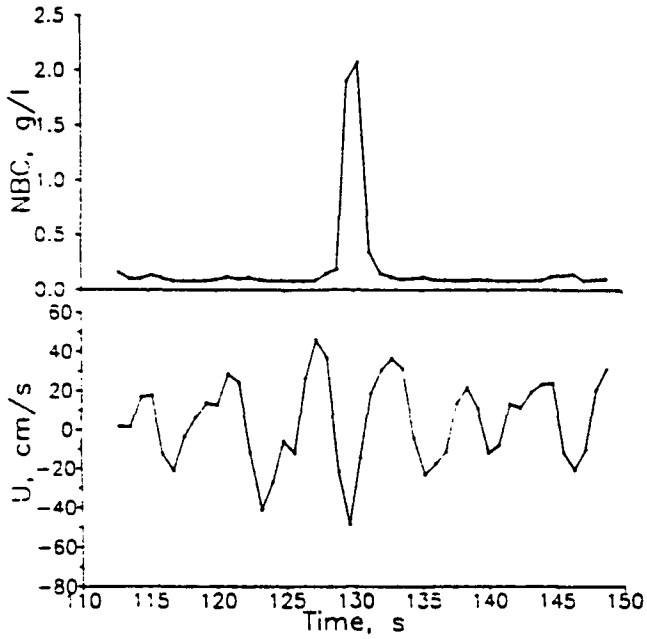

Fig. 7. Enlarged section of Fig. 3 illustrating an isolated suspension event that occurred in the midst of a group of larger waves.

NBC is increasing. The periods of rapidly increasing NBC occur more frequently while the cross-shore velocity is directed onshore than when the velocity is directed offshore. Because the peaks in onshore velocity were only slightly greater than the peaks in offshore velocity, this phenomenon cannot be explained in terms of a simple magnitude threshold. Comparing periods of equivalent magnitude onshore and offshore velocity, for example for $40 < |U| < 50$ cm/sec, the NBC during the onshore motion is a factor of 3.3 greater than during the offshore motion. Qualitatively similar observations were also made by Hanes and Huntley (1986) at a different field site using different instrumentation.

Hallermeier (1982), Sleath (1982), and Hanes and Huntley (1986) have suggested that fluid acceleration may be causally related to the concentration of suspended sand. For the present measurements, the correlation between water acceleration and

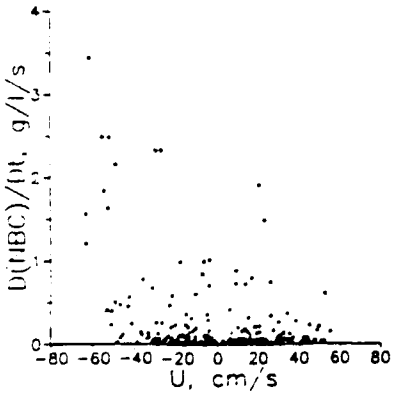

Fig. 8. Scatter plot of the rate of change of the NBC versus U for times when NBC was increasing.

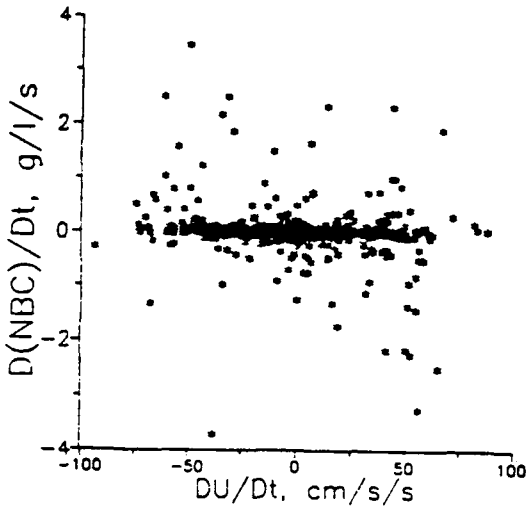

Fig. 9. Scatter plot of the rate of change of NBC versus the offshore fluid acceleration.

NBC was 0.084, which is barely significant at the 95 percent level. However, the anticorrelation between acceleration and the time rate of change of NBC is about twice as high (−0.164), as shown in Fig. 9. This supports the idea that water acceleration is significant to the entrainment of sand from the sea bed, but the low correlation is suggestive that the connection between acceleration and sand entrainment is moderated by other processes that have not yet been quantified.

5. Cross-Shore Sediment Transport

The correlation between high suspended sediment concentrations and shoreward fluid motion has a strong influence on the cross-shore sediment transport, resulting in a net shoreward transport of sediment during the measurement period. According to linear wave theory, there is little vertical structure in the wave induced fluid motions. The suspended sediment flux is therefore estimated at any depth as the concentration at that depth times the cross-shore fluid velocity measured at the current meter approximately 10 cm above the sea bed. Huntley and Hanes (1987) describe a method to correct the cross-shore velocity to crudely account for the bottom wave boundary layer, but found such a correction had little influence on the trends of the sediment transport. However, the results to be presented are subject to the caveat that the near-bed water velocity structure due to waves over a rippled bed have not been well documented in the field; there may be structure in the velocity field in the bottom 10 cm that we have not taken into account.

The NBC and estimated cross-shore suspended sediment flux can be described using the composite averaging technique. Figure 10 shows the results for the 20 events, where the four curves represent the composite averages of the NBC, the NBC plus one standard deviation, the fluid speed U, and the estimated cross-shore suspended sediment flux. The event initiates as the cross-shore velocity transitions from seaward to shoreward and the peak in concentration occurs while the velocity is directed shoreward. The concentration decreases as the fluid velocity direction reverses back to seaward motion. Although the average cross-shore velocity is

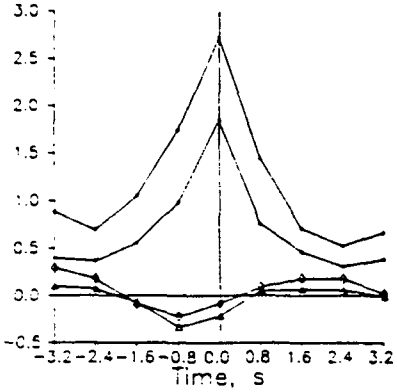

Fig. 10. Composite average of 20 events. The starred curves represent in grams per liter the NBC plus one standard deviation. The diamond curve is U in meters per second and the triangle curve is the estimated cross-shore sediment flux, in grams per 10 centimeters per centimeter per second.

directed seaward, the net flux during the event is directed shoreward because of the co-occurrence of the peak concentration with shoreward velocity.

Figure 11 shows the vertical profile of cross-shore sediment flux along with the profile of the product between the time averaged velocity and time averaged concentration. As pointed out by Jaffe, Sternberg, and Sallenger (1985) and Hanes and Vincent (1987), the fluctuation between the variations in concentration and velocity in a wave dominated environment are more significant to cross-shore transport than the product of the mean quantities. Although the 20 events identified earlier cumulatively only account for 35 percent of the record length, the cross-shore sediment transport during the events represents 82 percent of the total over the entire record. Amazingly, the 20 points corresponding to the peak concentrations of the 20 events account for 59 percent of the total transport, even though they occur during only 4 percent of the total measurement period.

Huntley and Hanes (1987) used standard time series analysis techniques to express the cross-shore flux in terms of the cospectrum of U and concentration. It is of interest to apply this methodology to these data, even though the transport is dominated by events. The cospectrum between U and NBC is shown in Fig. 12. The NBC spectrum is fairly broad, but the cospectrum exhibits a strong negative peak near the incident wave period, which corresponds to a shoreward transport of suspended sand.

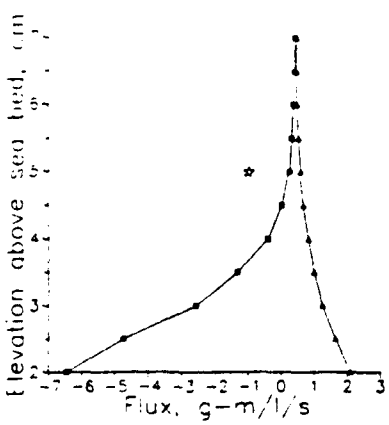

Fig. 11. Vertical profile of the time averaged cross-shore suspended sediment flux (squares) and the product of the time averages of U and C (triangles). The star represents the depth and time averaged flux.

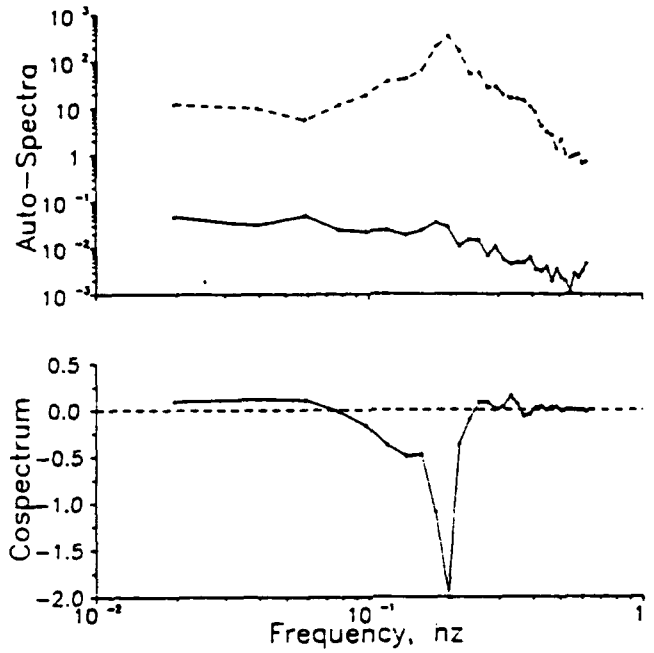

Fig. 12. The cospectrum of U and NBC, spectrum of U (dashed) and spectrum of NBC (solid). A negative cospectral value indicates shoreward transport.

6. Discussion

There are multiple processes consistent with these observations that are suggestive of rapid vertical entrainment of sediment from the sea bed. The precise form of this entrainment is not yet known. It may be a manifestation of the two-dimensional ejection and advection of sediment laden vortices due to the rippled bed, as seen for example in the laboratory by Sleath (1982). Alternatively, the event may be nearly one-dimensional, consisting of the vertical motion of a layer of sand, as modeled for example by Fredsoe, Andersen, and Silberg (1985). The scales of the events support the vertical entrainment scenario. If the events are considered to be the result of the horizontal advection of a vortex cloud of suspended sediment through the measurement area, then the duration of the event would be less than those observed. For example, using the measured vertical length scale of 5 cm as the length scale (L) of a cloud and the measured average horizontal fluid velocity (U) during the events of 6 cm/sec, then the time scale of the event would be order $L/U = 0.83$ sec, which is about a factor of 5 too low. It is of interest to note, however, that there were events with short time scales such as this on other days (Pescio and Hanes, 1988). If alternatively, sand were entrained from the sea bed and then settled back to the sea bed at a velocity W_0 of 2 cm/sec, the time scale would be approximately $2L/W_0 =$ 5 sec, which is consistent with the observations.

The intermittency of the events observed at this site is interesting and probably results from wave conditions that are near the threshold for sediment entrainment. The sequence of waves in a group appears to enhance suspension. This may be due to a hydrodynamic phenomena, which indicates that the vorticity induced near the sea bed during a wave half-cycle may not be fully cancelled by the oppositely directed vorticity induced in the successive half-cycle. Alternatively, these observa-

tions could result from the internal response of a porous bed to forcing by wave groups.

7. Concluding Remarks

The classical paradigm of suspended sediment in unidirectional flow in which the tendency of the sediment to sink is balanced by a vertically upward diffusive flux caused by fluid turbulence does not apply in wave dominated environments. This is not surprising because many investigators have described the organized process by which waves interact with a rippled bottom to form and eject sediment laden eddies. Even the casual swimmer can frequently notice the formation of either cloudy bursts of sediment, or a rising and falling sheet of sediment, depending on the wave and sea bed conditions.

Many new questions follow from the observation that suspension initiates during the shoreward phase of the fluid motion and that the net sediment transport resulting from this process is directed shoreward. For example, which features of the forcing are responsible for this asymmetry, is the process sometimes reversed, and does it occur across the inner continental shelf? Further observations of suspended sediment concentration, sea bed microtopography, and, if possible, fluid and sediment velocity at high resolution near the sea bed and within the sea bed would help to begin to answer some of these questions.

Acknowledgments

This work was supported in part by the U.S. Office of Naval Research, contracts N00014-86-K-0791 and N00014-89-J-1086, and the U.S. Geological Survey grant NA8611-D-S6068. I wish to thank Luc Pescio, who performed much of the original analysis that led to the identification of intermittent events.

References

Beach, R. A. and R. W. Sternberg, 1987. The influence of infragravity motions on suspended sediment transport in the inner surf zone of a highly dissipative beach. *Coastal Sediments '87*, ASCE, New York, pp. 913–928.

Brenninkmeyer, B. M., 1976. In situ measurements of rapidly fluctuating, high sediment concentrations. *Marine Geol.*, **20**, 117–128.

Daniel, P. E., 1986. Full data listing 1984, Stanhope Lane, Prince Edward Island, Report No. C2S2-23, National Research Council of Canada.

Downing, J. P., 1985. Suspended sand transport on a dissipative beach. In *Proceedings of the 19th Coastal Engineering Conference*, ASCE, New York, pp. 1765–1781.

Fredsoe, J., O. H. Andersen, and S. Silberg, 1985. Distribution of suspended sediment in large waves. *J. Waterway, Port Coastal, Ocean Div.*, **111** (6), 1041–1059.

Gillie, R. D., 1985. Canadian coastal sediment study final report, Report No. C2S2-17, National Research Council of Canada.

Hallermeier, R. J., 1982. Oscillatory bedload transport: Data review and simple formulation. *Continental Shelf Research*, **1**, 159–190.

Hanes, D. M., 1988. The significance of intermittent sediment suspension in the nearshore region. *Marine Geology*, **81** (No. 1), 175–183.

Hanes, D. M. and D. A. Huntley, 1986. Continuous measurements of suspended sand concentration in a wave dominated nearshore environment. *Continental Shelf Research*, **6** (No. 4), 585–596.

Hanes, D. M. and C. E. Vincent, 1987. Detailed dynamics of nearshore suspended sediment. *Coastal Sediments '87, New Orleans, Louisiana*. ASCE, New York, pp. 285–299.

Hanes, D. M., C. E. Vincent, D. A. Huntley, and T. E. Clarke, 1988. Acoustic measurements of suspended sand concentration in the C2S2 experiment at Stanhope Lane, Prince Edward Island. *Marine Geology*, **81** (No. 1), 185–196.

Huff, L. and D. C. Fiske, 1980. Development of two sediment transport systems. In *Proceedings of the 17th International Conference on Coastal Engineering*. ASCE, New York.

Huntley, D. A. and D. M. Hanes, 1987. Direct measurements of suspended sediment transport. *Coastal Sediments '87*, N. C. Kraus, ed. ASCE, New York, pp. 723–737.

Jaffe, B. E., R. W. Sternberg, and A. H. Sallenger, 1985. The role of suspended sediment in shore-normal beach profile changes. In *Proceedings of the 19th Coastal Engineering Conference*. ASCE, New York, pp. 1983–1996.

Pescio, L. and D. M. Hanes, 1988. Event analysis of local suspended sand concentration measurements. *Trans. A.G.U.*, **69** (No. 44), 1250.

Sleath, J. F. A., 1982. The suspension of sand waves. *J. Hydraulic Research*, **20**, 439–452.

Sternberg, R. W., N. C. Shi, and J. P. Downing, 1989. Continuous measurements of suspended sediment. In *Nearshore Sediment Transport*, Chap. 11A, R. J. Seymour, ed. Plenum, New York, pp. 231–257.

Thornton, E. B. and W. D. Morris, 1978. Suspended sediments measured within the surf zone. *Coastal Sediments '77*. ASCE, New York, pp. 655–668.

Young, R. A., J. Merrill, J. R. Proni, and T. L. Clarke, 1982. Acoustic profiling of suspended sediments in the marine boundary layer. *Geophys. Res. Lett.*, **9** (No. 3), 175–178.

Marine Geology, 94 (1990) 173–179
Elsevier Science Publishers B.V., Amsterdam — Printed in The Netherlands

Letter Section

A laboratory evaluation of optical backscatterance suspended solids sensors exposed to sand–mud mixtures

Keith A. Ludwig and Daniel M. Hanes*

Division of Applied Marine Physics and Ocean Engineering, Rosenstiel School of Marine and Atmospheric Sciences, University of Miami, 4600 Rickenbacker Causeway, Miami, FL 33149 (U.S.A.)

(Received October 16, 1989; revision accepted February 15, 1990)

ABSTRACT

Ludwig, K.A. and Hanes, D.M., 1990. A laboratory evaluation of optical backscatterance suspended solids sensors exposed to sand–mud mixtures. Mar. Geol., 94: 173–179.

Optical suspended solids sensors were studied in the laboratory in order to obtain calibration factors and evaluate the general behavior of the instrument when exposed to suspensions of mud and sand. The sensors were found to be capable of measuring the time-averaged concentration of either suspended sand or suspended mud, but the relative sensitivity of the sensor to these two different types of sediment varied by approximately an order of magnitude. In mixtures with a constant or known mud concentration, the instrument response to the mud may be treated as an offset, and gains appropriate to sand may be used to estimate the suspended sand concentrations. Semi-quantitative observations of the effects of flow direction relative to sensor orientation indicate that significant concern is warranted.

Introduction

Optical backscatterance suspended solids sensors have been used in the field in order to study the dynamics of suspended sediment in coastal regions (Downing et al., 1981; Sternberg et al., 1984; Hanes and Huntley, 1986). These sensors, manufactured by D&A Instruments and Engineering, emit infrared (IR) light, and measure the quantity of IR backscattered from a small (order of 10 cm^3) concentration-dependent volume immediately adjacent to the sensor face. Laboratory calibration allows conversion of this backscattered light intensity into suspended sediment concentration (Downing and Beach, 1989).

This paper describes laboratory tests designed to calibrate the sensitivity of the instruments to a variety of suspended sediments, and also to investigate the general behavior of the instruments. One of the important behavioral characteristics investigated in these experiments is the response of the instruments to sand in the presence of suspended mud. These tests were prompted by field investigations of the erosion of Louisiana barrier island shorefaces.

Sediments

Most of the sediments used in this study were collected at a field site near Fourchon, Louisiana, located southwest of New Orleans near Grand Isle. Both exposed beach sands and offshore bottom samples were collected at this location. The bottom samples were collected by

*Current address: Coastal and Oceanographic Engineering Department, University of Florida, 336 Weil Hall, Gainesville, Florida 32611

0025-3227/90/$03.50 © 1990 Elsevier Science Publishers B.V.

divers from approximately 2 km offshore, at an instrument deployment site in approximately 7 m of water. Examination of these bottom samples revealed silt, clay, and file sand with occasional shell fragments.

Following removal of the coarse shell fragments by seiving, size analysis indicated that more than 75% of the sediment was less than 20 μm in size. According to the "Glossary of Geology," mud, in the context of marine geology, is "a sticky, fine-grained, marine detrital sediment, either pelagic or terrigenous" (Bates and Jackson, 1980). As this definition aptly describes the Fourchon offshore bottom samples, throughout the remainder of this paper these samples shall be referred to as mud.

Fourchon sand samples were collected from the beachface on the exposed barrier island. The sand was rinsed, dried, and sieved through the following sieve stack (μm): 500, 355, 250, 180, 125, 90, 63, and a catch pan. Hereafter, the size of the sediment will reflect the sieve size in which the sediment was found.

Sand samples taken from two Florida locations were also used in some of the tests. The first of these locations is a beach approximately 1 mi north of Port Canaveral, near the city of Cape Canaveral, Florida. The second Florida location, chosen for its proximity to the laboratory, is a beach on the Virginia Key side of Bear Cut Inlet, located slightly east of Miami, Florida. Figure 1 shows the grain-size distributions for these sand samples. The mean and modal seive diameters (μm) are respectively, 191 and 187 for Fourchon, 289 and 237 for Bear Cut, and 247 and 172 for Cape Canaveral.

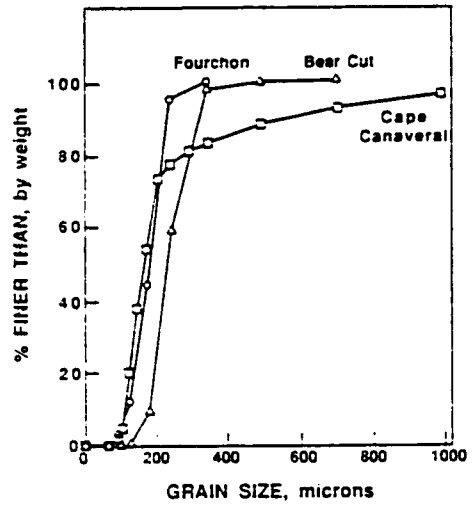

Fig. 1. Beach sand size distributions.

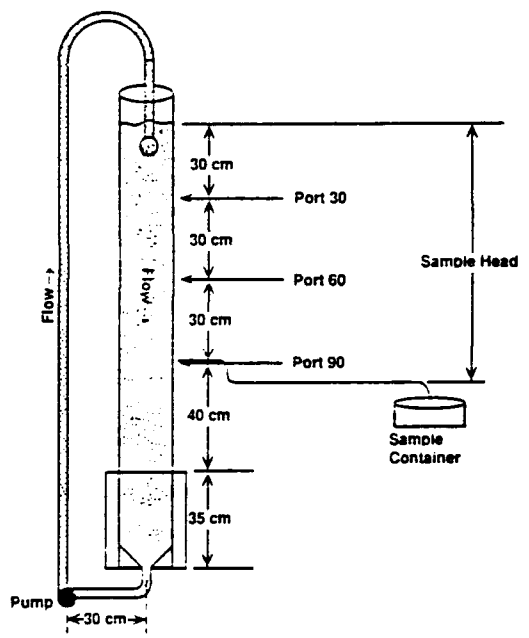

Fig. 2. Scheme of recirculation calibration facility, including water-sampling apparatus.

Calibration facility

The primary test apparatus for this study consists of a recirculation calibration tank (Fig. 2) containing 46 l of water and sediment circulated at an average speed of 2.2 cm/s in the test area. The water and sediment flow downward through the test section and are recirculated with a centrifugal pump. The discharge passes through a diffuser at the top of the tank in order to thoroughly mix the sediment. The test section of the tank consists of a vertical clear acrylic tube with ports through which water samples may be drawn. These ports are located 30, 60, and 90 cm below the full mark of the tank. The hydraulic head difference be-

tween the top of the tank and the discharge end of the clear nylon tube drives the water-sampling process.

The tank was designed to allow for the creation of a uniform and known concentration of suspended sediment. No attempt was made to simulate any particular hydraulic conditions which might be found in a field situation. Effects such as the dependence of calibration coefficients on Reynold's number will not be addressed, although concerns related to flow direction will be presented later in this paper.

The ability to create suspensions of known concentration was verified through physical sampling of the water–sediment mixture. Samples of approximately 2 l were drawn through the $\frac{1}{4}$ in tube and passed through a 63 μm sieve which trapped the sediment. Prior to further discussion of these samples, the following definitions will be introduced:

Input concentration: The dry weight of sediment placed in the tank (g) divided by the volume of water placed in the tank (l).

Sampled concentration: The dry weight of sediment sampled (g) divided by the volume of water sampled (l).

Actual concentration: The dry weight of sediment suspended in the test section (g) divided by the volume of water (l).

β: The ratio of the sampled concentration to the input concentration.

In a uniformly mixed suspension with no sediment settling onto surfaces, the input concentration is equal to the actual concentration. This is indeed the case, as will be shown below.

When water samples are draw through a tube oriented perpendicular to the mean flow direction, the resulting sampled concentration is expected to be slightly lower than the actual concentration. In a similar sampling apparatus, Bosman (1982) found that when the sampling velocity exceeds the mean test section flow, the ratio of sampled concentration to actual concentration approaches a value of 0.73. Water sample velocities obtained in the present tests varied with the elevation of the discharge end of the sampling tube. At a level of 30 cm below the initial tank level, a sample velocity of 85 cm/s is obtained. At 90 cm below the initial tank level, the sample velocity increases to 160 cm/s. In all cases the velocities greatly exceed the cross-sectionally averaged flow velocity of 2.2 cm/s.

Tests were conducted to assess the possible dependence of the sampled concentration on the vertical location of the sample intake, the cross-sectional location of the sample intake (1), the input concentration of sediment, and the flow rate. The results of all these tests appear in Tables 1–3. None of these variables has a significant and consistent effect on the β coefficient. The fact that β is about 0.85, rather then 0.73 as found by Bosman, is probably due to the flow intake geometry. However, the value of β is not significant to the reminder of the results; these tests were simply performed to verify that the tank was well mixed. There-

TABLE 1

β versus vertical location and sample flow rate

	Sample head		
	30 cm	60 cm	90 cm
Port 30	0.83	0.95	0.80
Port 60	0.93	0.83	0.88
Port 90	0.88	0.85	0.85

Input concentration = 1.0 g/l.
Port number indicated distance (cm) below full level.
Intake at center of tank.

TABLE 2

β versus input concentration

Conc. (g/l)	β
0.05	0.55
0.10	0.80
0.50	0.82
1.0	0.85
5.0	0.79
10.0	0.78

Port 90.
Head 90 cm.
Intake l = 9.5 cm.

TABLE 3

β versus l

l (cm)	β
1.27	0.89
9.50	0.85
9.50	0.83
14.60	0.85

Port 90.
Head 90 cm.
Input Conc. = 1.0 g/l.

fore, the input concentration may be assumed to be equal to the actual concentration. This is believed to be a valid assumption for all the tests, independent of sediment type or size, and is a desirable feature of the recirculation tank.

Because the fluid in front of the sensor face is in constant motion, it is reasonable to assume that there will be a variation in concentration with respect to time. Physical samples indicate that when this variation is averaged over approximately 1 min, the resulting sampled concentration becomes steady, and representative of the input concentration. Similarly, time averaging of the OBS signal also yielded a steady mean voltage, which may then be equated with the input concentration.

Results and discussion

In order to test the response of OBS sensors to suspended beach sand, measurements were taken using the three different sands at several concentrations ranging from clear water to 10.0 g/l. In clear tap water the signal fluctuations were approximately equal to the resolution of the analog-to-digital converter, about 5 mV. Although the gains and offsets vary between sensors, each sensor is quite linear over the range of concentrations considered. Each sensor has an adjustable gain, so the difference between sensor gains is superfluous to this discussion. The correlation coefficients typically exceed 0.99. An example of the results of these tests for Fourchon beach sand appears in graphical form in Fig. 3. The complete list of gains is given in Table 4.

An important consideration in the deployment of these sensors at a field site which contains sands of varying sizes is the dependence of the response on the sediment size. The response to different grain sizes was examined by seiving the Fourchon beach sand into size classes of 63, 90, 125, 180 and 250 μm and a mixture which approximated the natural distribution. The mean grain size of the mixture was 183 μm.

Figure 4 shows the gain versus mean size of each size fraction for sensors 1 and 4. For each sensor, gains for sands ranging in size from 63 to 355 μm differ from the gain of the mixture by a maximum of about 17%. The variation with size is not monotonic, presumably be-

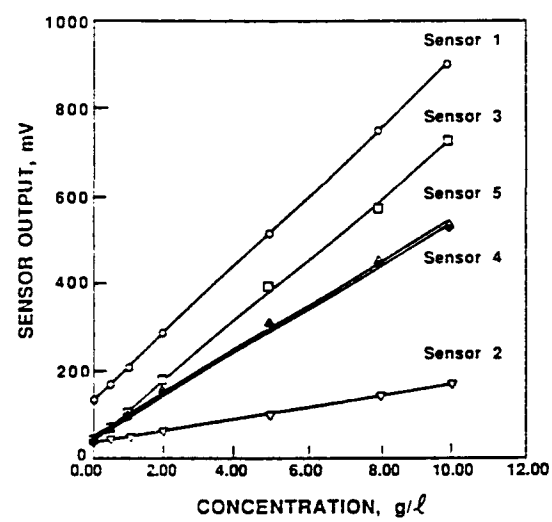

Fig. 3. Response to Fourchon beach sand.

TABLE 4

Gains for the various sediments

	Sieved mud	Fourchon sand	Canaveral sand	Bear Cut sand
Sensor 1	686.1	76.5	93.5	98.5
Sensor 2	115.1	12.8	15.5	21.8
Sensor 3	522.4	67.6	84.8	84.7
Sensor 4	484.6	50.4	69.4	71.9
Sensor 5	594.5	50.5	69.3	78.4

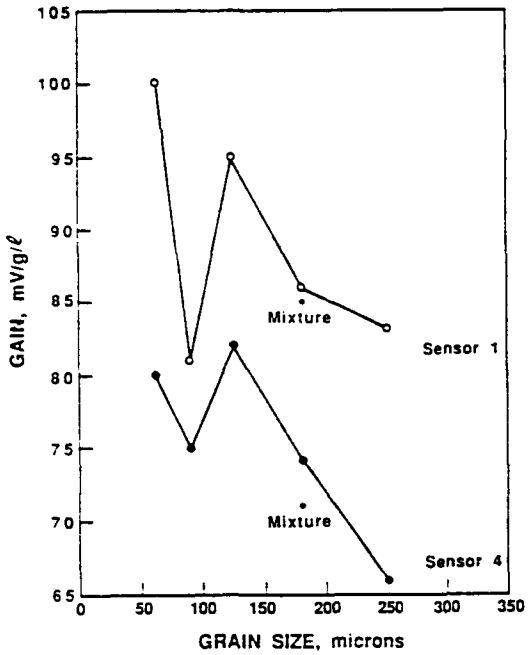

Fig. 4. Gain of sensors 1 and 4 as a function of sand size.

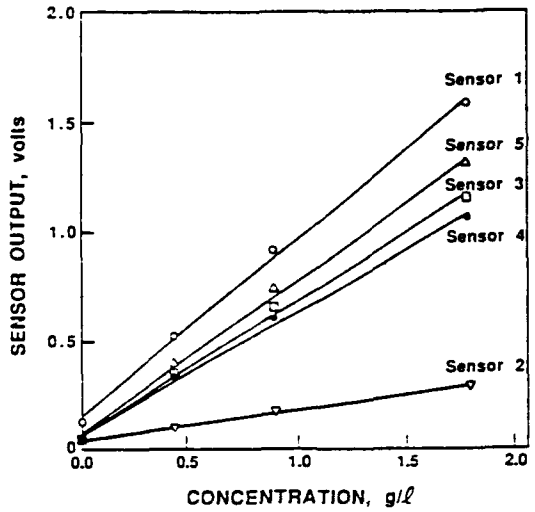

Fig. 5. Response of all five sensors to moderate concentrations of Fourchon mud.

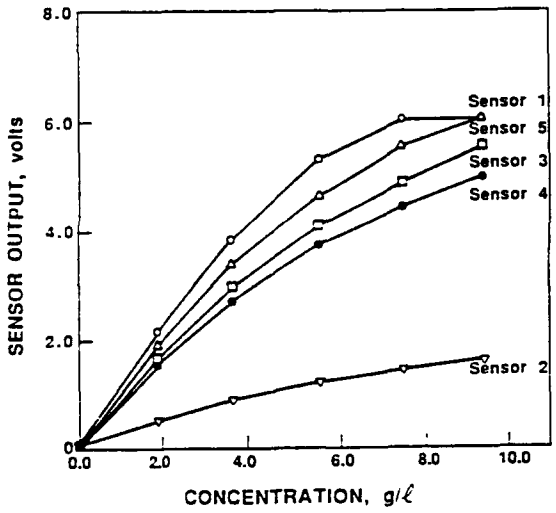

Fig. 6. Response of all five sensors to high concentrations of Fourchon mud.

cause of the differing mineralogies of the various size fractions: the 63 μm size group appears nearly black in color, suggesting high concentrations of magnetite and hornblende, while the tan coloration of the groups over 125 μm suggests compositions of largely quartz and feldspar.

Two series of tests were conducted using suspended mud. The first series determined calibration gains and offsets for the range of concentrations anticipated in the field. The concentrations of mud used in these tests were 0.0, 0.45, 0.9 and 1.8 g/l. Results for each sensor appear in graphical form in Fig. 5 and in tabular form in the "sieved mud" column of Table 4. A second series of tests investigated the behavior of these instruments over their entire measurement range. These concentrations were started at approximately 2 g/l and increased in 2 g/l steps until sensor one, the most sensitive sensor, registered nearly the same voltage for two successive steps. The final concentration was approximately 10 g/l. Figure 6 contains the results of this series of runs for all five sensors. The instrument response to mud is linear up to concentrations of approximately 3 or 4 g/l. These gains are nearly ten times as great as those determined previously for sand. At higher concentrations, the sensitivity decreases, although not markedly. Finally, at high concentrations which depend on the resistor settings for the particular sensor, the sensor will saturate and become insensitive to further increases in concentration.

In order to recreate a condition similar to

that expected at the Louisiana field site, various sand concentrations are studied in two different mud backgrounds. The concern is the ability of the sensors to "see" the sand through a background mud signal. The background mud concentrations have values of 0.0, 0.9 and 1.8 g/l. Tests are run on these backgrounds alone and with these backgrounds in combination with concentrations of Fourchon beach sand. The sand concentrations are 0.5, 1.0, 2.0 and 5.0 g/l.

The results of these runs appear in Fig. 7 and in Table 5. The "change %" column of Table 5 contains the percentage change of the preceeding gain as compared to the gain for zero mud background. The gains of sensors 1 and 5 remain constant to within 1 % regardless of the mud background. Sensors 2 and 4, however, show drops in gain of the order of 10 % for both mud backgrounds as compared to sand-only concentrations. Stranger still is the behavior of sensor 3. The gain experienced by this sensor drops 11.8 % for the first mud background and recovers to within 3.8 % for the higher mud background. We have no explanation for the difference in behavior between the sensors. Although these results are not perfectly consistent, they do show that mud backgrounds of this magnitude reduce the gain by factors in the range of 10 % or less.

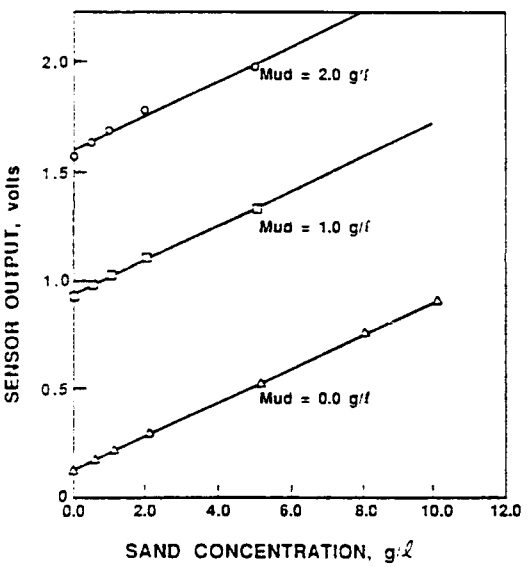

Fig. 7. Response of sensor 1 to sand in the presence of various mud backgrounds.

TABLE 5

Gains for Fourchon sand in various mud backgrounds

	Mud = 0 g/l	Mud = 0.9 g/l		Mud = 1.8 g/l	
	Gain	Gain	Change %	Gain	Change %
Sensor 1	76.55	76.50	−0.1	76.20	−0.5
Sensor 2	12.83	11.62	−9.4	10.84	−15.5
Sensor 3	67.62	59.20	−11.8	65.04	−3.8
Sensor 4	50.44	46.14	−8.5	44.77	−11.2
Sensor 5	50.52	50.40	−0.2	50.74	−0.4

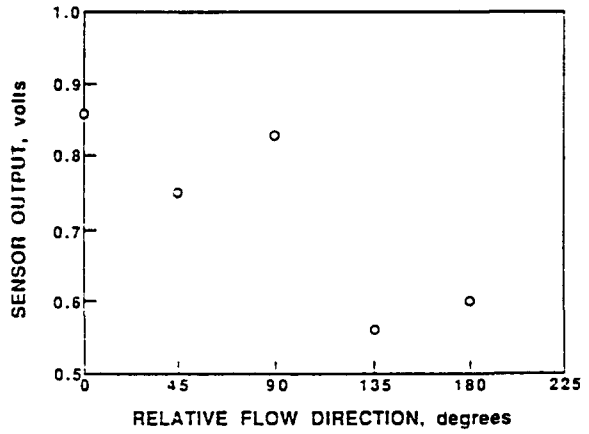

Fig. 8. Sensor 1 output as a function of sensor orientation relative to the mean flow direction. Angle of zero corresponds to flow directly toward the sensing face of the instrument.

A series of experiments examined the sensor response as a function of the orientation of the sensor relative to the direction of the flow. For these experiments, 5.0 g/l of Bear Cut sand was input and sensor 1 was positioned 25 cm below the water surface. The diffusion nozzle was removed from the discharge hose in an attempt to obtain a high-energy unidirectional flow field. No sand was observed accumulating on any part of the sensor, regardless of the orientation of the sensor. Figure 8 indicates that the measured concentration varies with sensor orientation. The magnitude of the variations reach as much as 50%. The results are believed

to result from the flow pattern around the sensor.

Conclusions

The following conclusions may be drawn. The sensors possess a very linear response for concentrations of sand between 0.0 and at least 10 g/l. and mud between 0.0 and 2.0 g/l. The sensor sensitivity to suspended mud is significantly higher than that due to sand. At high mud concentrations, a non-linear calibration curve is required. For mixtures of mud and sand, the sensor responds linearly to the concentration of each component, with the gains for such mixtures being comparable to those which would apply to each component alone.

The size of the sand in suspension does not greatly affect the gain of the sensors. This is true for the grain-size distribution and related composition of the sand found at the Fourchon beach site. A more consistent dependence of gain on size might be expected in a more mineralogically uniform sand sample.

Use of these instruments for the measurement of suspended sand in areas which concurrently experience suspended mud is not recommended, for two reasons. First, in order to avoid saturating the sensors with mud during high-energy events (these are typically the events of most interest), the instrument gain must be set so low that high resolution of sand suspension is prevented. Second, during times when the mud concentration varies, it is unclear how a distinction should be drawn between the portion of the return due to suspended sand and the portion of the return due to suspended mud.

Although the flow direction dependence tests do not attempt to duplicate conditions expected in the field, they do indicate that a significantly strong dependence probably exists. This is especially true in the wave-dominated environments of the nearshore, where the flow direction is frequently changing. For deployment in wave-dominated environments it is recommended that the sensors be oriented such that the wave-induced flow is parallel to the sensor face. Further testing, preferably in a larger tank with a more controlled flow structure, is highly recommended.

Acknowledgements

We wish to acknowledge the financial support of the United States Geological Survey, passed through Florida Sea Grant, the Naval Civil Engineering Laboratory, and the U.S. Office of Naval Research. We also with to thank Bruce Jaffe for his technical assistance.

References

Bates, R.L. and Jackson, J.A., 1980. Glossary of Geology. Am. Geol. Inst., Falls Church, Va., 2nd ed.

Bosman, J.J., 1982. Concentration measurements under oscillatory water motion. Delft Hydraul. Lab. Rep. M 1695, Part II, pp. 5–10.

Downing, J.P. and Beach, R.A., 1989. Laboratory apparatus for calibrating optical suspended solids sensors. Mar. Geol., 86: 243–249.

Downing, J.P., Sternberg, R.W. and Lister, C.R.B., 1981. New instrumentation for the investigation of sediment suspension processes in the shallow marine environment. In: C.A. Nittrouer (Editor), Sedimentary Dynamics of Continental Shelves. Mar. Geol., 42: 19–34.

Hanes, D.M. and Huntley, D.A., 1986. Continuous measurement of suspended sand concentration in a wave dominated nearshore environment. Cont. Shelf Res., 6: 585–596.

Sternberg, R.W., Shi, N.C. and Downing, J.P., 1984. Field investigation of suspended sediment transport in the nearshore zone. In: Proc. Coastal Eng. Conf., Am. Soc. Civ. Eng., New York, pp. 1782–1798.

Marine Geology, 96 (1991) 1–18
Elsevier Science Publishers B.V., Amsterdam

Acoustic measurements of suspended sand on the shoreface and the control of concentration by bed roughness

Christopher E. Vincent[a], Daniel M. Hanes[b*] and Anthony J. Bowen[c]

[a]*School of Environmental Sciences, University of East Anglia, Norwich NR4 7TJ, U.K.*
[b]*Rosenstiel School of Marine and Atmospheric Sciences, University of Miami, Miami FL 33149, U.S.A.*
[c]*Department of Oceanography, Dalhousie University, Halifax, N.S., Canada*

(Revision accepted July 3, 1990)

ABSTRACT

Vincent, C.E., Hanes, D.M. and Bowen, A.J., 1991. Acoustic measurements of suspended sand on the shoreface and the control of concentration by bed roughness. Mar. Geol., 96: 1–18.

Acoustic backscatter measurements of the concentrations of sand in suspension on the shoreface, seawards of the breaking zone, during a mild storm event show that sand concentrations increase initially but then rapidly decrease as the wave energy increases: it is suggested that the bed roughness is a major control on suspended sand concentration and that the decrease in concentration is due to decreasing ripple steepness after the break-off bed shear stress is exceeded. No direct measurements of bedforms were available and the combined wave-current interaction model of Grant and Madsen (J. Geophys. Res., Vols. 84 (1979) and 87 (1982)) with extensions to movable bed roughness (ripple dimensions from Carstens et al's. 1969 laboratory data (U.S. Army Corps Eng. CERC Tech. Mem. 28) and to sediment-induced self-stratification (Glenn and Grant, J. Geophys. Res., Vol. 92, 1983) was used to predict the current and suspended sand concentration profile. Matching the measured and modeled concentrations at 2 cm above the bed, the values of the resuspension coefficient γ_0 were found to decrease as excess skin friction increased, in a manner similar to that suggested by Drake and Cacchione (Cont. Shelf Res., Vol. 9, 1989) but were an order of magnitude larger. Using the much smaller ripple dimensions of Nielsen (J. Geophys. Res., Vol. 86, 1981) changed the model results very little. Significant differences were found between the time-averaged suspended sand profiles and those predicted by the model.

Sand transport fluxes have also been computed using the instantaneous products of measured suspended concentrations and currents (the current being the sum of steady and wave-induced components). The wave-induced fluxes show considerable variability from run to run but the general pattern is of a transport profile having a shoreward maximum at 5–10 cm above the bed and offshore transport in the few centimetres closest to the bed: little net transport occurred above 15 cm. These fluxes show a weak dependence on the wave energy, becoming more shoreware and the height of the maximum shoreward transport decreasing as the wave energy increased, again consistent with the influence of the ripple steepness.

1 Introduction

Most of us are familiar with the temporal changes which occur on beaches. Storms and other periods of high wave activity tend to move sand offshore: beach levels drop and the land behind the beach becomes more vulnerable to wave attack, to erosion or to flooding. During fair weather, often referred to as "summer wave conditions", a gradual accretion occurs and beach levels rise. These shorter term changes are often accompanied by more gradual changes in beach volume or position which may be due to alterations in sand supply to the beach (natural or man-induced) or to changes in the wave climate.

Such qualitative descriptions of how beaches alter mask the problems which exist in quantifying the processes which are responsible for such changes. The alongshore transport of sand driven by waves breaking on the shoreface at an angle can result in changes in beach levels if there is a

*Present address: Coastal and Oceanographic Engineering, University of Florida, Gainsville, FL 32611 (U.S.A.).

0025-3227/91/$03.50 © 1991 — Elsevier Science Publishers B.V.

flux divergence along the beach. However, most of the rapid changes in beach volumes are due to the cross-shore transport of sand; sand is transported from the upper beach face out to bars beyond the breaker zone and beach levels may be reduced by many tens of centimetres in the course of a single storm.

The data described here were collected as part of the C-COAST field experiment designed to investigate the hydrodynamic and sediment transport processes on beaches. The Canadian Coastal Sediment Transport Program (C-COAST) is a combined project of the Universities of Toronto, Dalhousie and Memorial and is sponsored by the National Science and Engineering Research Council of Canada. The results presented here are from a single acoustic concentration meter (ACM) and two electromagnetic current meters mounted close to the sea bed 100 m from the mean water mark during a field experiment on Queensland beach, Nova Scotia, during October 1987. Results from the other instrumentation recording concurrently will be presented elsewhere.

2 Queensland beach and the experimental design

Queensland beach is a small sandy pocket beach some 300 m wide, enclosed by rocky headlands. To the south it opens into a larger bay which itself opens to the Atlantic Ocean (Fig.1). Atlantic swell and storm waves penetrate through the bay opening, arriving as long-crested waves almost normal to the beach. The beach profile is a simple one with an upper shore face slope of 5° at mean water level (MWL), decreasing to 1.7° 100 m offshore (Fig.2). A surficial sand sample collected by divers 100 m offshore close to the ACM had a modal size of between 2.5 and 3.0ϕ when dry sieved through half-phi sieves (Fig.3).

Instrumentation, consisting of electromagnetic current meters, optical backscatter probes (OBS), acoustic concentration meters (ACM) and pressure sensors, was mounted on bottom frames 60, 70, 90 and 100 m from MWL (Fig.2). All were shore connected and, with the exception of the ACMs, the data were recorded on the Dalhousie University UDATS system (Hazen et al., 1988). Because of their high data return rate the ACMs recorded directly on their own PC-based logging systems. The ACM data presented here also recorded two "slow" channels of data taken from the UDATS system to ensure exact temporal sychronisation between the different logging systems.

The ACM was mounted 60 cm above the sea bed with its transducer axis vertical on the horizontal arm of an H-frame 100 m from MWL

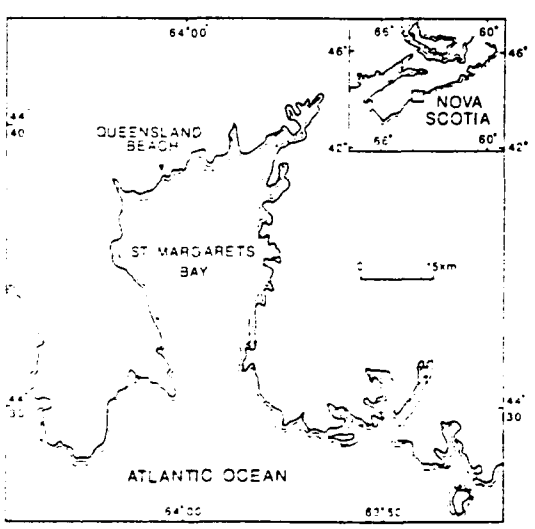

Fig.1. Location of Queensland beach, Nova Scotia.

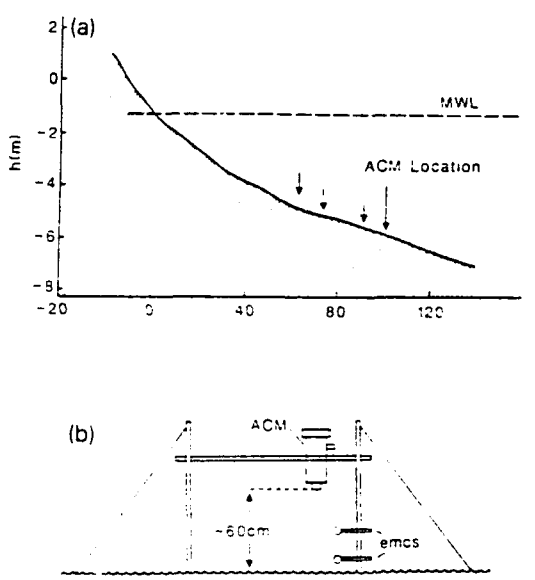

Fig.2. (a) Cross section of Queensland beach with the four major instrument locations. (b) H-frame with acoustic concentration meter (ACM) and electromagnetic current meters (EMCS).

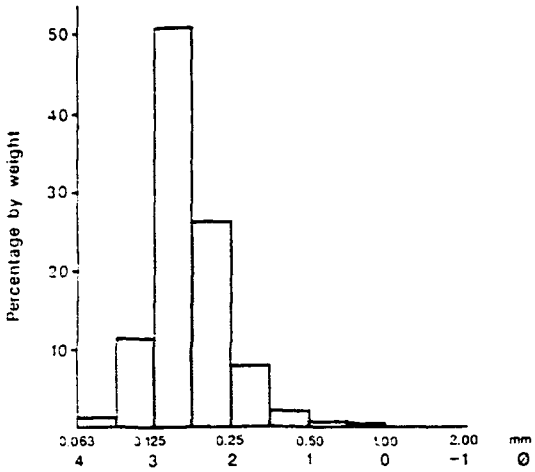

Fig.3. Sieved sand size distribution in half phi intervals of surficial sample taken from Queensland beach close to the ACM location.

(Fig.2). Current meters were fixed to one of the vertical arms of the frame at heights of 20 cm and 50 cm above the bed so that they measured the current close to the area ensonified by the ACM.

The instrumentation was positioned by divers who also made visual observations of bottom roughness and ripple wavelength whenever possible. A video camera was mounted near the 90 m frame and recordings made of resuspension events, but no direct information about ripple dimensions could be gathered for this storm due to poor visibility and low light levels.

3 The acoustic measurement of suspended sediment

3.1 The acoustic concentration meter

The acoustic concentration meter (ACM) used in this field experiment is similar to that described by Huff and Fiske (1980), Hanes et al. (1988) and Libicki et al. (1989). The acoustic frequency is 2.8 MHz and the pulse length is about 10 μs. Range gating the backscattered acoustic signal allows the sediment concentration profile to be estimated at 124 range "bins", with a vertical resolution of 0.81 cm. The pulse repetition rate was 10 Hz and four profiles were averaged before storing the data on disk together with two values from "slow" channels, on this occasion two components of an electromagnetic current meter. Disk access time and other software constraints meant that one average profile was recorded every 0.58 s. 1250 average profiles (12 min) were recorded during each run.

3.2 Calibration of the ACM

The ACM was calibrated in a laboratory recirculation tank (Vincent et al., 1986) using sand taken from the beach at Queensland. The calibration curves for sand at four concentrations are shown in Fig.4a, the digital value of the nominal voltage (8 bit, 0–255 scale) plotted against distance. The concentrations are those measured by withdrawing a water sample from the centre of the recirculation tank and then filtering and weighing the filtrate. These calibration profiles are each an average of 1250 individual profiles. The acoustic backscatter intensity V^2 (expressed here in terms of the notional voltage V seen by the system) from a uniform field of scatterers of concentration $C(r)$ is assumed to be an inverse function of range r with corrections for attenuation due to water and to the scatterers:

$$V^2 = Br^{-2}C(r)\exp\left\{-4\alpha r - \int_0^r \beta C(r)\,\mathrm{d}r\right\} \qquad (1)$$

where B is a constant which includes the beam strength and sediment backscattering cross section, α is the attenuation due to water and β is the attenuation of the beam due to the presence of sediment. Here we assume a value of 1.1 dB/m for the absorption of 2.8 MHz sound by seawater and that β is 2.5×10^{-5} cm^{-1} (mg l^{-1})$^{-1}$ (Sheng and Hey, 1988). B depends on the acoustic power emitted by the transducer, the sediments in the water column and the gain of the receiver circuits. For this calibration (using Queensland sand) a value of 6.4×10^4 (mV^2 cm^2 mg^{-1} l) was found to fit the calibration data best. Normalising the backscattered acoustic energy using the above equation reduces the calibration data to that shown in Fig.4b: the region close to the transducer (5–25 cm) corresponds to the near-field region and fits the theoretical extent of the near field well (ka^2, where k is the acoustic wavenumber and a is the radius

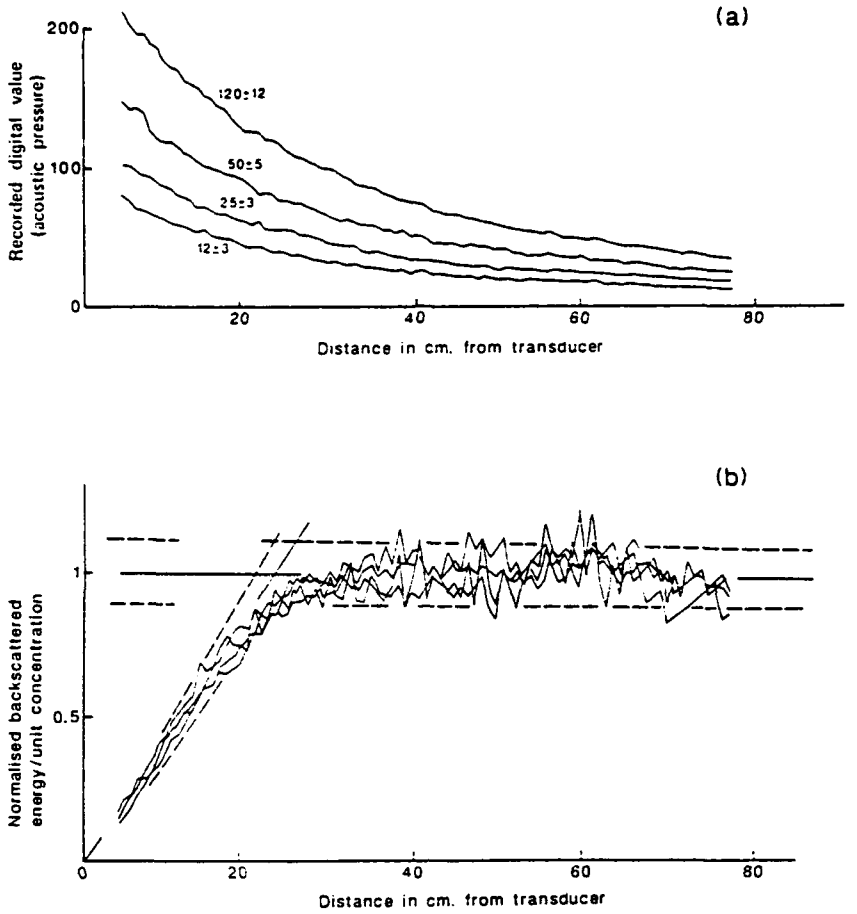

Fig.4. (a) Calibration curves for sand from Queensland beach in a recirculation tank for four concentrations. (b) Normalised backscatter signal intensities from the four calibration curves above. The near-field extends to 25 cm. Dashed lines are ±10% of the normalised value.

of the transducer). The field data are converted to concentrations using a step wise application of eqn. (10) with a linear correction in the near-field region as indicated in Fig.4b.

3.3 Limitations of the ACM

There are limitations to the effective use of the ACM for measuring rapid changes in the concentration of sediment above the sea bed (Vincent et al., 1986). Breaking waves inject bubbles into the water column and, as air bubbles have a high acoustic impedance, the ACM can clearly "see" them but it is difficult in any quantitative manner to differentiate between suspended sand and air bubbles; hence the ACM should not be used near the surf zone. At high suspended concentrations, difficulties can also be encountered because the acoustic beam is attenuated so rapidly that distance with little energy penetrates to the full range of the ACM; at 100 mg l^{-1} the attenuation is 0.6 db m^{-1} but provided high concentrations (> 1 g l^{-1}) are encountered only within a few centimetres of the sea bed, reasonable estimates of the concentration can still be made.

3.4 Sensitivity to particle size

Calibration tank tests with sieved sands suggest that an ACM operating at 2.8 MHz is most sensitive to sands between 1.0 and 1.5ϕ (0.5–0.35 mm). The calibration equation described

above assumes that the size distribution of the suspended sediment is always the same as that of the surficial sample collected. In the field the size distribution will vary both spatially and temporally so the calculation of the suspended concentration from the backscattered acoustic intensity may involve considerable uncertainty. The magnitude of this uncertainty cannot, therefore, be precisely quantified but for sand sizes which are much less than the wavelength of the sound (which is 0.58 mm at 2.8 MHz): halving the sand size halves the intensity of the backscattered signal.

3.5 Organic material in suspension

A further confusion in the interpretation of an ACM record was highlighted during a pre-storm trial of the instrumentation. Wave heights were very low (< 10 cm) and divers had reported that only occasional sediment suspension was occurring from the top of ripples on the sea bed. Visual monitoring of the ACM signal during this period showed clear and regular acoustic returns from the lowest 5 cm of the water column, returns which varied in intensity over a wave period as would be expected from sediment resuspension by waves. A further inspection of the sea bed beneath the ACM by one of the authors revealed that there was a layer of fine organic material floating close to the sea bed and being advected through the ACM beam by the wave motion. Spatial variations in the density and thickness of this organic material were seen by the ACM as a temporal variation in suspended concentration equivalent to a sand suspension of about 100 mg l^{-1} in the lowest 3–5 cm of the water column.

There is little that can be done to eliminate this problem as in many circumstances it will not be known if organic material is present in the water. During the deployment described below we expect the organic material to be dispersed more uniformly through the water column than in the situation described above. It should also be noted that a uniform suspension will appear as a signal in the transport due to the mean current but should integrate to zero for wave-induced transport, assuming the particles move with the water.

3.6 Accuracy and precision of the ACM measurements

Because of the likely variation in the sand size distribution with height above the sea bed it has not been possible to calculate the accuracy of the suspended sand concentrations: Vincent and Green (1990) show that the apparent concentrations above the sea bed under waves decreased faster than predicted by the Glenn and Grant (1983) model and suggested that this was due to finer material diffusing higher into the flow. During the Queensland experiment, suspended sand samples were taken at a number of heights above the botton near the 90 m size using a Nielsen suction sampler: there was some indication of a decrease in the model size of suspended sand but the differences were small (Greenwood, 1989, pers. commun.). The precision of the measurements is believed to be high and the calibration curves suggest a precision of $\pm 10\%$ in the assessment of the sand concentration, equivalent to the calibration sand size distribution.

4 Acoustic measurements of suspended sand concentrations during a mild storm event

4.1 Wave and current conditions

The event chosen for analysis was a 25 h period of onshore winds beginning at 0800 h on 28th October 1987 (Julian days 301–302). During this period, twenty 12 min runs of the ACM were recorded, of which sixteen had synchronous electromagnetic current meter (EMCM) data; runs are identified by Julian day plus a sequence number (301/1–301/13, 302/1–302/7). Examples of the temporal and spatial variations in the suspended sand concentrations during four runs (301/3, 301/11, 302/1 and 302/5) are shown in Fig.5 together with the EMCM current speeds. Mean currents, wave-induced currents and wave period for the complete period are summarised in Table 1.

Speeds from the shore-normal component of the EMCM at 20 cm above the bed (waves were approaching directly onto the shore) were used to calculate the wave-induced current and the wave period: no significant difference was found between the speeds measured by the EMCMS at

20 cm and 50 cm. Mean currents, speed and direction, were calculated from the two components of the EMCM at 20 cm. The method of analysis follows that used by Vincent and Green (1990). After subtracting the mean current, the wave period is found from the downward zero-crossing period. The maximum current is then found for each wave half-cycle and a "significant current" (defined in a similar way to the significant wave height, as the average of the highest one-third of the maximum currents) is identified for the onshore half-cycles and for the offshore half-cycles of the wave (Table 1).

4.2 Position of the sea bed

Suspended sand concentrations decrease rapidly away from the bed so an accurate assessment of

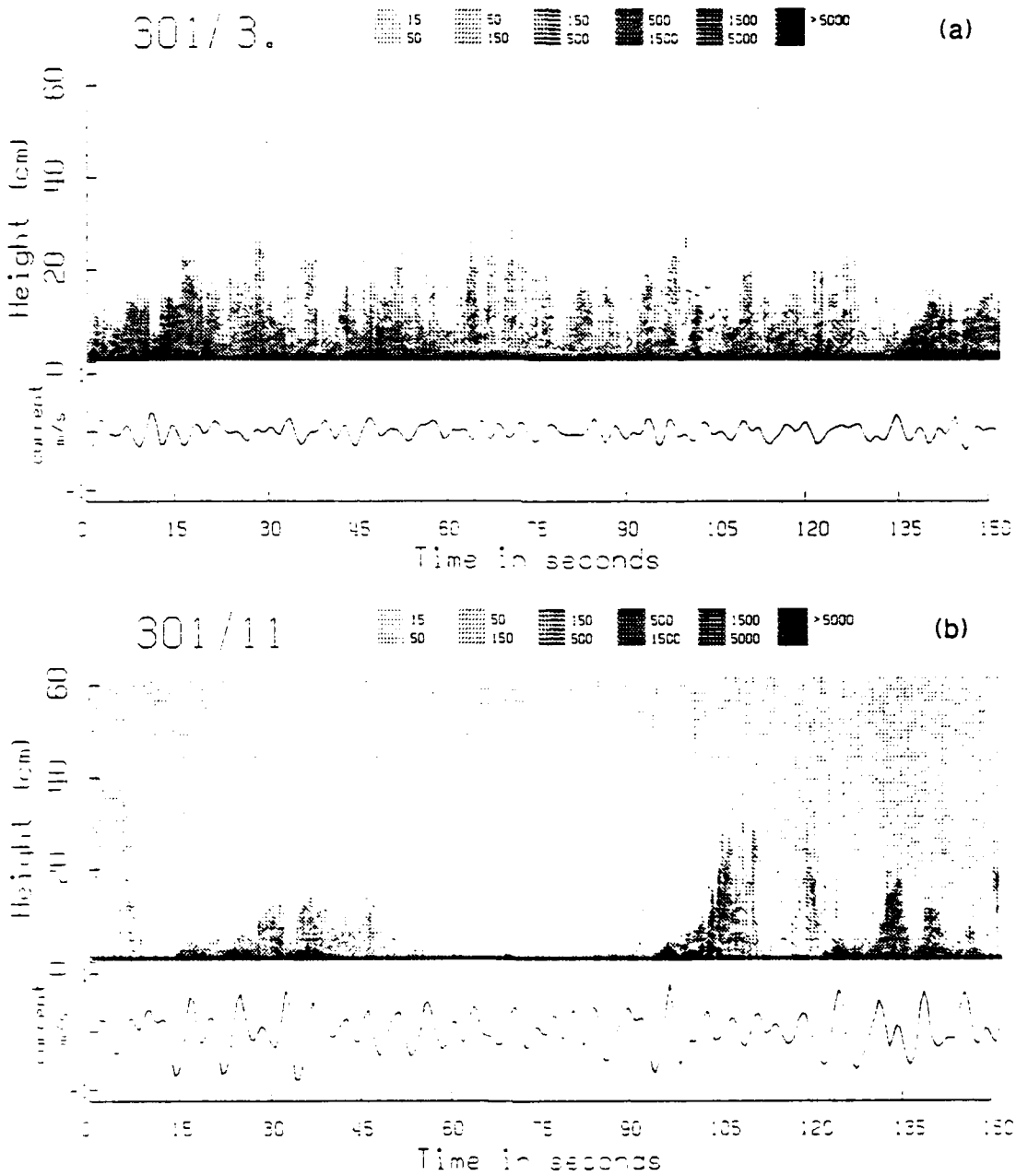

the position of the sea-bed is required. The level of maximum acoustic backscatter was interpreted as an echo from the sea bed: this level remained constant (± 1 bin, ± 0.8 cm) throughout each run, indicating that any bed features present were not moving significantly during that time, or that the amplitude of the bedforms was small (~ 1 cm). The acoustic footprint of the ACM is about 3.5 cm at the 60 cm range (defined by the position of the -20 db intensity contour of the acoustic beam).

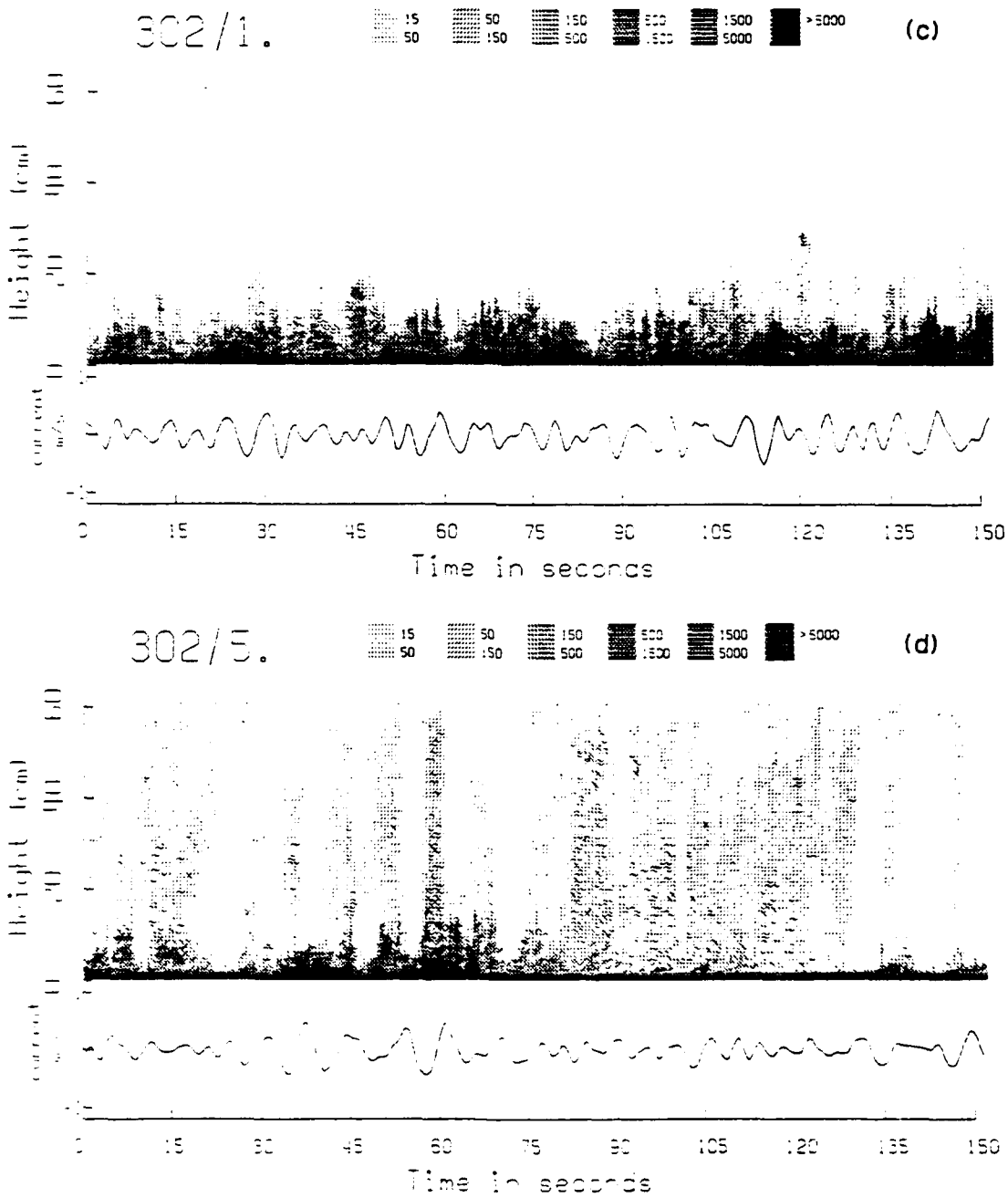

Fig.5. Grey-scale plots of the suspended sand concentrations (mg/l) and the current speed (in the cross-shore direction) for four bursts. (a) 301/3, (b) 301/11, (c) 302/1, (d) 302/5.

TABLE 1

Wave and current conditions during the 24 h mild storm event, showing the mean currents and the significant (sig) and average (av) wave-induced maximum currents for the onshore and offshore half-cycles (in cm s^{-1}). Bursts for which sychronous current data were not available are shown with asterisks

Burst No.	Time (h)	Mean currents (cm s^{-1})		Wave-induced currents				Wave period (s)
		On/off	Along	Onshore		Offshore		
				sig	av	sig	av	
301/1*	0815	2.6	−1.1	25	16	−27	−16	4.70
301/2*	0900	2.6	−1.1	25	16	−27	−16	4.70
301/3	1100	2.3	−0.6	24	15	−24	−15	4.36
301/4*	1300	3.1	−1.6	30	19	−31	−19	4.60
301/5	1530	4.1	−1.9	39	26	−40	−25	4.73
301/6*	1645	4.1	−1.9	39	26	−39	−25	4.74
301/7	1730	5.8	−2.8	52	35	−52	−32	4.92
301/8	1830	4.8	−1.6	58	39	−56	−35	4.95
301/9	1930	7.5	−4.3	61	39	−55	−34	4.95
301/10	2030	9.1	−5.8	73	48	−67	−40	5.12
301/11	2130	6.8	−3.7	61	40	−57	−35	5.08
301/12	2200	6.0	−3.8	62	40	−58	−37	5.34
301/13	2330	5.7	−3.2	50	32	−47	−30	5.54
302/1	0130	4.2	−2.0	37	23	−37	−23	5.10
302/2	0230	2.8	0.5	43	25	−41	−23	5.85
302/3	0330	2.6	0.7	37	24	−36	−22	6.12
302/4	0530	2.3	1.2	40	26	−39	−25	6.30
302/5	0630	2.0	0.9	32	20	−30	−19	5.91
302/6	0730	2.7	1.2	37	25	−33	−21	6.40
302/7	0850	2.9	1.2	38	24	−34	−21	6.38

A time series of bed heights from the individual profiles of run 301/8 ($\Delta T = 0.58$ s) and profiles smoothed over ten pulses ($\Delta T = 5.8$ s) is shown in Fig.6.

Over the period of the storm event however, the run-average sea bed position varies over more than 4 cm (Fig.7) but it is not possible to conclude how much of this variation is due to local erosion or deposition, or to the position of bedforms relative to the acoustic beam axis.

4.3 *Run-average suspended sand concentrations*

The concentrations of sand in suspension vary rapidly from second to second, producing a picture of complex suspension events (Fig.5). Time averaging the concentration profiles over the period of a run showed an unexpected pattern of suspended

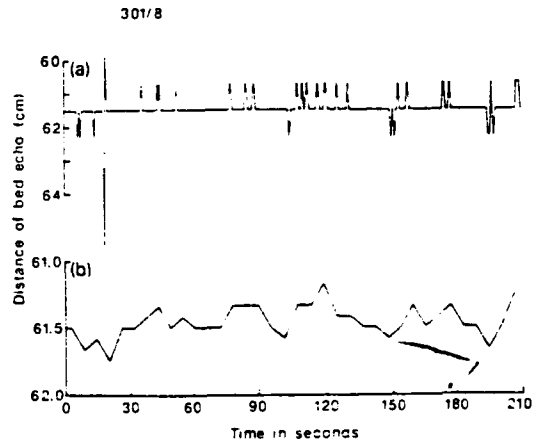

Fig.6. (a) Time series of the position of the sea bed, identified by the maximum echo strength for the first 210 s of burst 301/8 ($\Delta T = 0.58$ s). (b) Time series averaged over ten profiles ($\Delta T = 5.8$ s).

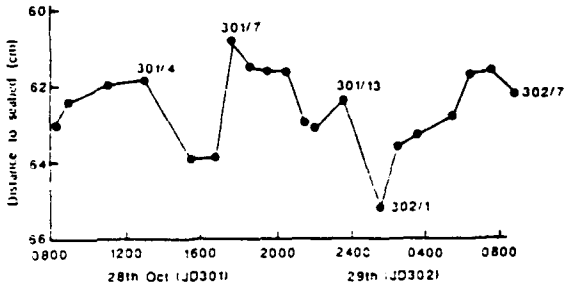

Fig.7. Burst-averaged positions of the sea bed over the period of the storm.

sand concentrations, with the lowest concentrations apparently associated with the period of highest waves (shown here by the largest wave-induced current speeds). A time series of run-averaged concentrations at four heights (2.5, 5, 12 and 25 cm) together with the wave-induced current speed and wave period is shown in Fig.8. There is a negative correlation, significant at 99%, between the significant wave orbital speed and concentrations at 2.5, 5 and 12 cm.

Three average run-mean profiles have been plotted in Fig.9 for periods when profile shape was not changing rapidly: the rising phase of the storm (301/1–301/4), the maximum wave height phase (301/7–301/12) and the waning phase (302/2–302/7). These average profiles differ from

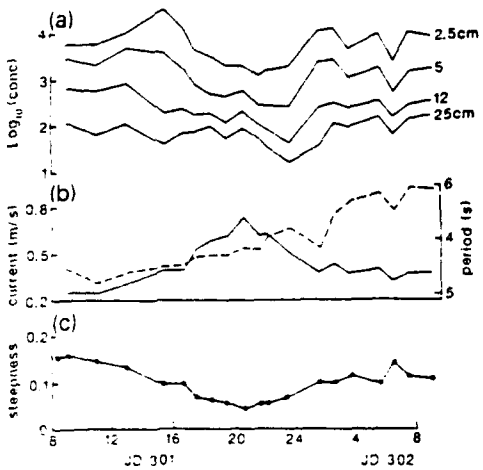

Fig.8. (a) Burst-averaged suspended sand concentrations at 2.5, 5, 12 and 25 cm above the sea bed (note the log scale). (b) Significant wave-induced currents (solid line) and the wave periods (dashed line). (c) ripple steepness from Carstens et al. (1969).

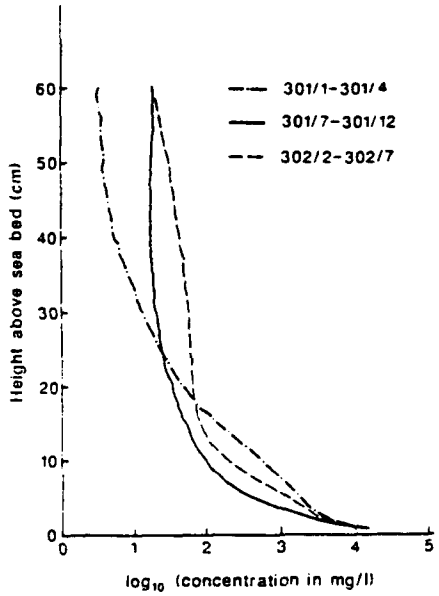

Fig.9. Average profiles for 301/1–301/3 (the rising storm), 301/6–301/11 (maximum wave heights) and 302/2–302/7 (the waning storm).

each other at most heights but the important differences are in the lowest 20 cm; above this level, much of the backscatter may be due to suspended organic material (see later).

5 Wave–current interaction, bed roughness and the resuspension of sand

Under a combination of a steady current and oscillatory flows, which are generated near the sea bed by surface waves, an interaction occurs between the waves and the currents. Close to the sea bed there is a shallow wave boundary layer while above this the steady current experiences an apparent roughness which is enhanced by the presence of the waves (Grant and Madsen, 1979). We have used the model developed by Grant and Madsen (1979, 1982) and Glenn and Grant (1983) for the wave–current interaction over a mobile bed, including the suspension of sand and a correction for any sediment-induced self-stratification which may occur (this model is henceforth referred to as the Grant–Madsen–Glenn or GMG model), to predict the combined flow characteristics and the bedforms. We have also compared the concentration measured 2 cm above the sea bed with that

predicted by the model. The model integrates the Smith and McLean (1977) expression for the reference concentration $C(z_0)$ over a wave period T:

$$C(z_0) = \frac{1}{T} C_b \int_{t=0}^{t=T} \frac{\gamma_0 S'(t)}{1 - \gamma_0 S'(t)} \, dt \tag{2}$$

where C_b is the bed volume concentration of sediment, γ_0 is an empirical constant, z_0 is the roughness height in the wave boundary layer and $S'(t)$ is the instantaneous normalised excess skin friction, defined as:

$$S'(t) = \frac{|\tau'(t)| - \tau_{cr}}{\tau_{cr}} \tag{3}$$

where $\tau'(t)$ is the instantaneous skin friction and τ_{cr} is the critical shear stress for initiation of motion. Various authors have suggested different values for γ_0 (Dyer, 1980; Wiberg and Smith, 1983; Hill et al., 1988; Vincent and Green, 1990) and recently Drake and Cacchione (1989) presented data which showed that γ_0 decreased rapidly as excess skin friction increased.

The steady current profile for non-stratified conditions applicable to all the data presented here, both within ($z < \delta_w$) and above ($z > \delta_w$) the wave boundary layer, is given by:

$$U(z) = (U^2_{*c} \; \kappa U_{*cw}) \ln(z/z_0), \; z < \delta_w \tag{4}$$

$$U(z) = (U_{*c} \; \kappa) \ln(z/z_{0c}), \; z > \delta_w \tag{5}$$

where $z_0 = k_b/30$ and k_b is the hydrodynamic roughness, and z_{0c} is the apparent roughness that retards the mean flow above the wave boundary layer. The friction velocity characteristic of $z > \delta_w$ is $U_{*c} = (|\tau_c| / \rho)^{0.5}$, where τ_c is the time-averaged instantaneous shear stress at the top of the boundary layer. $U_{*cw} = (|\tau_{cw}| / \rho)^{0.5}$ is the friction velocity applicable for $z < \delta_w$, where τ_{cw} is the maximum instantaneous boundary shear stress.

The neutral concentration profile is:

$$C(z) = C(z_0)(z/z_0)^{-\alpha}, \; z < \delta_w \tag{6}$$

$$C(z) = C(z_{0c})(z/z_{0c})^{-\alpha}, \; z > \delta_w \tag{7}$$

where α is the suspension parameter:

$$\alpha = \gamma w_f / \kappa U_{*cw} \text{ for } z < \delta_w \tag{8}$$

$$\alpha = \gamma w_f / \kappa U_{*c} \text{ for } z > \delta_w \tag{9}$$

w_f is the sand fall velocity and γ is an empirical constant set to 0.74 following Businger et al's. (1971) work in the atmospheric boundary layer.

The ripple geometry is defined empirically from the laboratory data of Carstens et al. (1969). The ratio of the maximum Shields parameter ψ' over a wave cycle to the critical Shields parameter ψ_c is used to define the break-off point where the ripple steepness begins to decrease:

$$(\psi'/\psi_c)_B = 1.8 \, S_*^{1.6} \tag{10}$$

S_* is a dimensionless sediment parameter given by:

$$S_* = (D/4\nu)[(s-1)gD]^{0.5} \tag{11}$$

where ν is the kinematic viscosity, s is the specific gravity of sand, g is the acceleration due to gravity and D is the sediment diameter. The Shields parameter is defined in the usual way as:

$$\psi = \tau / \rho(s-1)gD \tag{12}$$

where τ is the appropriate bed shear stress (the skin friction) and ρ is the density of seawater. The ripple heights η (from table 1 in Grant and Madsen, 1982) are given by:

$$\eta/a = 0.22 \, (\psi'/\psi_c)^{-0.16} \text{ for } (\psi'/\psi_c) < (\psi'/\psi_c)_B \tag{13}$$

$$\eta/a = 0.48 \, S_*^{0.8} \, (\psi'/\psi_c)^{-1.5} \text{ for } (\psi'/\psi_c) > (\psi'/\psi_c)_B \tag{14}$$

where a is the wave orbital excursion amplitude. The ripple lengths λ are:

$$\lambda/\eta = 6.25 \, (\psi'/\psi_c)^{0.04} \text{ for } (\psi'/\psi_c) < (\psi'/\psi_c)_B \tag{15}$$

$$\lambda/\eta = 3.6 \, S_*^{-0.6} \, (\psi'/\psi_c) \text{ for } (\psi'/\psi_c) > (\psi'/\psi_c)_B \tag{16}$$

We have run the GMG model using the wave and current data from the EMCMs: the onshore significant wave-induced current was used to represent the wave conditions in each run. The model was allowed to define its own equilibrium bedform conditions and to correct for any self-stratification (no significant sediment stratification was encountered during any of the runs presented here and all the results are effectively for neutral conditions). Table 2 shows the ripple height η, wavelength λ and steepness η/λ, the values of U_{*c}, U_{*cw}, z_{0c} and z_0 and the excess skin friction predicted by the model, the last term based on the assumption that

TABLE 2

Predicted bedforms, friction velocities and roughness lengths from the Grant–Madsen–Glenn model for each run, and the normalised excess bed friction

Burst No.	Bedforms			δ_w (cm)	U'_{*c} (cm/s)	U'_{*cw} (cm/s)	z_{0c} (cm)	z_0 (cm)	Normalised excess skin friction	γ_0
	η (cm)	λ (cm)	η/λ							
301/1	3.3	21	0.16	4.2	0.64	8.0	3.6	0.48		
301/2	3.3	21	0.16	4.2	0.64	8.0	3.6	0.48		
301/3	3.4	22	0.15	4.4	0.57	8.0	3.8	0.51	0.5	9.7
301/4	3.9	27	0.14	5.4	0.91	9.3	4.3	0.54		
301/5	2.6	28	0.093	5.2	1.05	8.6	3.6	0.25	2.4	4.6
301/6	2.6	28	0.093	5.2	1.05	8.6	3.6	0.25		
301/7	1.7	31	0.056	5.6	1.38	9.0	3.2	0.14	4.6	0.72
301/8	1.5	31	0.047	6.0	1.21	9.5	3.7	0.13	5.7	0.50
301/9	1.3	31	0.042	6.2	1.82	9.9	3.1	0.13	6.5	0.35
301/10	1.0	33	0.030	7.6	2.42	11.7	3.4	0.14	7.6	0.20
301/11	1.4	32	0.042	6.4	1.69	9.9	3.3	0.13	6.4	0.17
301/12	1.4	34	0.042	6.5	1.64	9.9	3.5	0.13	6.5	0.27
301/13	2.1	35	0.061	6.3	1.47	8.9	3.4	0.17	4.1	0.46
302/1	3.2	31	0.[illegible]	5.7	1.13	8.8	3.9	0.32	2.0	0.29
302/2	3.1	37	.100	6.6	0.80	8.8	4.9	0.26	2.8	1.70
302/3	4.2	38	0.110	7.1	0.84	9.1	5.5	0.44	1.9	1.63
302/4	3.8	[illegible]	0.097	7.2	0.81	9.0	5.5	0.36	2.3	1.95
302/5	5.0	36	0.140	7.2	0.73	9.6	6.0	0.67	1.2	1.54
302/6	4.4	40	0.110	7.5	0.91	9.2	5.7	0.47	1.8	2.16
302/7	4.2	40	0.105	7.4	0.95	9.1	5.5	0.43	2.0	1.84

the average skin friction over ripples is the same as for that over a flat bed (Grant and Madsen, 1982).

5.1 Variations in γ_0

The values of γ_0 shown in Table 2 are the values required by the model to match the predicted suspended sand concentration at 2 cm above the sea bed with the measured values (average of concentrations from bins 2 and 3 above the bed). A reference concentration at 2 cm is preferred to that at 1 cm because of the uncertainty of ± 1 bin (± 0.8 cm) in the bed position; however, the strong concentration gradient near the bed will mean that $C(z_0)$ is very sensitive to the matching height chosen. The variation in γ_0 with excess skin friction is shown in Fig.10: the trend is similar to that found by Drake and Cacchione (1989) but the

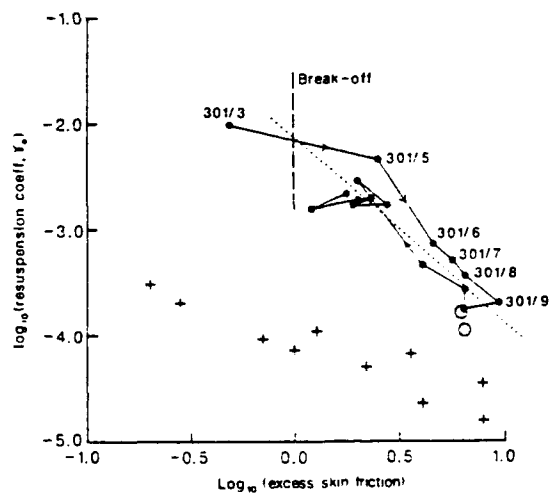

Fig.10. Plot of the variation in the resuspension coefficient γ_0 against the maximum (over one wave period) excess skin friction. ● This study; ○ Vincent and Green (1990); + Drake and Cacchione (1989).

values of γ_0 are generally an order of magnitude higher. Drake and Cacchione's values, however, were extrapolated from nephelometer data taken at a height of 1.9 m over a silt bed with a mean grain size of 16–25 μm. Towards the end of the storm period when wave heights were decreasing and bed roughness was greatest, the values of γ_0 were close to the value of 2×10^{-3} found by Smith and McLean (1977) in the Columbia River. During the higher excess skin friction period the values were very close to those measured by Vincent and Green (1990) for resuspension on a beach with similar-sized sand.

5.2 *Comparison of modelled and observed concentration profiles*

There are important differences, similar to those noted by Vincent and Green (1990), between the average concentration profiles and the concentration profiles predicted by the GMG model (Fig.11). In particular, the observed gradients of suspended sand are steepest close to the bed (in the wave boundary layer), whereas the model predicts a much more uniform gradient close to the bed. Also, it is difficult to identify any position as the top of the wave boundary layer in the observed profiles.

While these fundamental differences in the profile shapes show that the GMG model does not satisfactorily predict the average naturally occurring sand concentration profiles in this nearshore environment, the model's shortcomings are not unexpected. The GMG model is a two-layer model with the vertical eddy diffusivity being time-invariant and linear with height: it uses a single wave height, wave period, ripple height and ripple length. A real sea has a spectrum of wave heights and periods so the height of the wave boundary layer will vary from wave to wave, the ripples too are likely to be responding dynamically to the changing wave characteristics and vortex ejection *per se* cannot be considered because of the form of the eddy diffusivity profile. The differences do nevertheless warn of problems in using the GMG model to predict suspended sand concentration profiles.

6 On–offshore suspended transport rates

The transport of sand can be divided into two components, an advective term and a wave oscillatory term. The advective component of transport is due to the steady (time-averaged) current $\bar{U}(z)$ and the entire suspension of sand in the water is bodily transported. In the wave oscillatory component, where the net transport of water is by definition zero, sand transport occurs due to time lags between fluctuations in the current $U_w(z,t)$ and fluctuations in suspended sand concentrations $C(z,t)$. While the instantaneous current can be divided easily into steady and wave oscillatory components, $U(z,t) = U_w(z,t) + \bar{U}(z)$, it should be noted that the same cannot be done for the suspended sand concentration in any meaningful way: the sand concentration at any instant is due to the

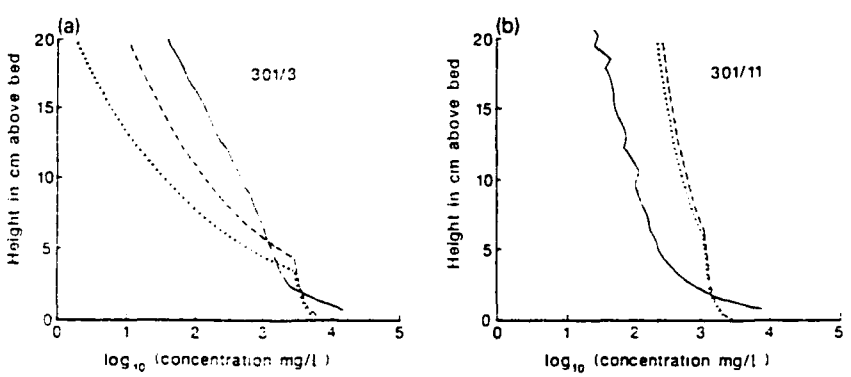

Fig.11. Comparison between the measured burst-averaged concentration profiles (solid lines) and those predicted using the GMG model with ripple dimensions determined from Carstens et al. (1969) (dashed lines) and from Nielsen (1981) (dotted lines) for bursts 301/3 and 301/11.

excess skin friction due to both waves and currents (alongshore as well as on–offshore) over a mobile bed formed by the combined system. Nevertheless, it is useful to compute the relative importance of the two components, as defined below.

The on–offshore component of the transport of suspended sand, averaged over the period of a burst, has been calculated in several ways, as follows:

(1) For steady currents, as a function of height above the bed ($Q(z)_{mean}$) and integrated over the water column (Q_{mean}):

$$Q(z)_{mean} = \bar{U}(z)\,\bar{C}(z) \tag{17}$$

and

$$Q_{mean} = \sum_{z=\text{sea bed}}^{z=20\,\text{cm}} Q(z)_{mean} \tag{18}$$

where $\bar{C}(z)$ is the burst-mean concentration profile.

(2) For the wave oscillatory currents, again as a function of height from the bed ($Q(z)_{wave}$) and integrated over the water column (Q_{wave}):

$$Q(z)_{wave} = \sum_{t=0}^{t=\text{burst}} \overline{u_w(z,t)C(z,t)} \tag{19}$$

and

$$Q_{wave} = \sum_{z=\text{sea bed}}^{z=60\,\text{cm}} Q(z)_{wave} \tag{20}$$

The average velocity profile was that predicted by the GMG model with neutral stratification matched with the measured currents at 20 cm. This also assumes that the current measured at 20 cm is in the potential flow region. Closer to the bed in the wave boundary layer, the current velocity at height z is given by:

$$U_w(z,t) = \left(1 - \frac{ker\,2\sqrt{\xi} + i\,kei\,2\sqrt{\xi}}{ker\,2\sqrt{\xi_0} + i\,kei\,2\sqrt{\xi_0}}\right) \times U_w(\infty,t) \tag{21}$$

where $U_w(\infty,t)$ is the wave-induced current outside the wave boundary layer, $\xi_0 = z_0/l$ and $\xi = z/l$ where $l = \kappa U_{wcw} T/\pi$, and *ker* and *kei* are Kelvin functions of the first order (Grant and Madsen, 1978). This equation shows the phase of the current changing towards the sea bed: the magnitude of this change is about 20° at 1 cm, less than the time resolution of the measurements (0.58 Hz) for most waves, so no attempt was made to correct for phase shift in these results.

6.1 *Vertically integrated transport*

The vertically integrated values of Q_{mean} and Q_{wave}, which describe the total sand transport (flux) past the measurement position, divided into the two components described above, are shown in Fig.12. The steady currents have an offshore component throughout the experimental period so the transport due to the steady current Q_{mean} is offshore throughout. The transport due to the wave oscillatory term Q_{wave} is of a similar magnitude to Q_{mean} but is generally directed towards the shore; the uncertainty limits shown are those which would result from an error of ±1 bin in selecting the position of the sea bed. There is considerable variability in the transport flux from run to run although the general trend is for the flux to become

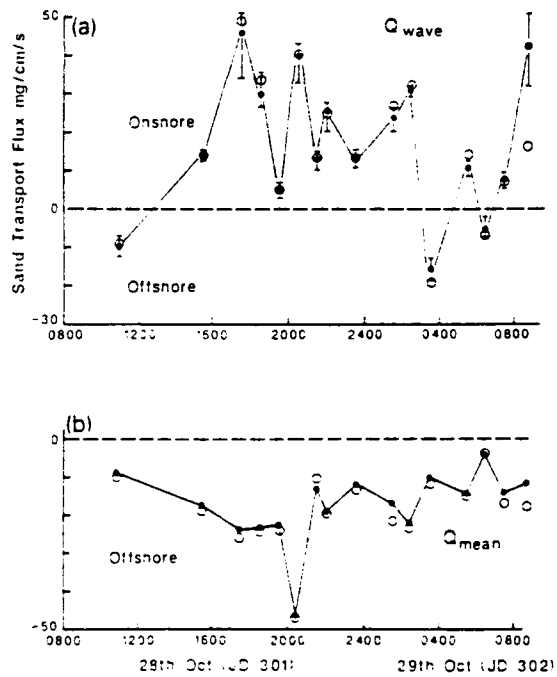

Fig.12. Vertically integrated values of the cross-shore sand transport due to the steady current (Q_{mean}) and to the waves (Q_{waves}) using the GMG model with ripple dimensions from Carstens et al. (1969) (●) and from Nielsen (1981) (○). The range of Q_{wave} shown on the Carstens values are those for an uncertainty of ±1 bin.

more negative (shorewards) with the larger waves. The variability results partly from the flux being the resultant of large transports in opposite directions (gross transport is an order of magnitude larger than the net transport) but also from the groupiness of the waves: the influence of groupiness can be seen in Table 3 where the on–offshore flux has been calculated for each third of run 302.2.

6.2 *Transport profiles*

For each run the vertical profiles of suspended sand $Q(z)_{wave}$, $Q(z)_{mean}$ and the total transport $Q(z)_{total}$ in the on-offshore direction have been computed. Marked changes occur during the course of the storm, particularly in the heights at which maximum wave transport $Q(z)_{wave}$ is observed. With the exception of the last three runs (302.4–302.7), very little wave-induced transport occurs above 20 cm: the steady transport above 20 cm observed in a number of runs is probably due to contamination of the backscattered signal by suspended organic material. Figure 13 shows a sequence of suspended transport profiles from every other run for the lowest 20 cm. The wave component $Q(z)_{wave}$ (cross-hatched for clarity) is shorewards for all except the first profile (run 301.3), and has a peak transport elevation which decreases with height as the waves increase in height. During the final four runs (302.4–302.7) transport occurs to a much greater height from the bed ($\sim$50 cm), although still decreasing with height: this may be due to the efficient ejection of vortices from the ripple crests (predicted to be steep at this time) or perhaps to patchy organic material in suspension (see Fig.5d).

6.3 *Sensitivity of the transport estimates*

The sand transport values computed here clearly depend on the form of the current profile (both wave-induced and the steady component) chosen to occur below the EMCM at 20 cm. All the above results use the GMG model which includes ripple dimensions based mainly on laboratory experiments by Carstens et al. (1969). However, Nielsen (1981) noted that natural ripples, while obeying essentially the same rules as laboratory ripples, were shorter and less steep due to the irregularity of natural waves (Fig.14). To investigate the sensitivity of the results presented hitherto to the exact form of the current below 20 cm we have tried a number of forms for the profile, based on both the GMG model generating its own ripple dimensions (Carstens et al., 1969) and also on the model run with ripples defined from Nielsen (1981) for irregular waves alone:

$$\lambda/a = \exp \frac{693 - 0.37 \ln^8 M}{1000 - 0.75 \ln^7 M}$$

$$\eta/a = 21\, M^{-1.85}$$

where a is the wave semi-excursion and M is a mobility number defined as

$$M = (a\omega)^2/(s-1)gD$$

TABLE 3

Variation in the gross and net vertically integrated sand flux due to the waves during run 302.2 (values in parentheses are ranges). Three 240 s long segments, their wave-induced current speed and period are shown together with values for the complete run

Time period (s)	Wave current (cm/s)			On–offshore flux (mg/cm/s)	
	Onshore	Offshore	Period	Gross	Net
0–240	30	33	5.2	170 (19)	23 (25)
241–480	44	40	6.0	503 (47)	48 (49)
481–720	51	46	6.7	650 (84)	91 (89)
0–720	43	40	5.8	442 (49)	52 (55)

more negative (shorewards) with the larger waves. The variability results partly from the flux being the resultant of large transports in opposite directions (gross transport is an order of magnitude larger than the net transport) but also from the groupiness of the waves: the influence of groupiness can be seen in Table 3 where the on–offshore flux has been calculated for each third of run 302.2.

6.2 *Transport profiles*

For each run the vertical profiles of suspended sand $Q(z)_{wave}$, $Q(z)_{mean}$ and the total transport $Q(z)_{total}$ in the on-offshore direction have been computed. Marked changes occur during the course of the storm, particularly in the heights at which maximum wave transport $Q(z)_{wave}$ is observed. With the exception of the last three runs (302.4–302.7), very little wave-induced transport occurs above 20 cm: the steady transport above 20 cm observed in a number of runs is probably due to contamination of the backscattered signal by suspended organic material. Figure 13 shows a sequence of suspended transport profiles from every other run for the lowest 20 cm. The wave component $Q(z)_{wave}$ (cross-hatched for clarity) is shorewards for all except the first profile (run 301.3), and has a peak transport elevation which decreases with height as the waves increase in height. During the final four runs (302.4–302.7) transport occurs to a much greater height from the bed ($\sim$50 cm), although still decreasing with height: this may be due to the efficient ejection of vortices from the ripple crests (predicted to be steep at this time) or perhaps to patchy organic material in suspension (see Fig.5d).

6.3 *Sensitivity of the transport estimates*

The sand transport values computed here clearly depend on the form of the current profile (both wave-induced and the steady component) chosen to occur below the EMCM at 20 cm. All the above results use the GMG model which includes ripple dimensions based mainly on laboratory experiments by Carstens et al. (1969). However, Nielsen (1981) noted that natural ripples, while obeying essentially the same rules as laboratory ripples, were shorter and less steep due to the irregularity of natural waves (Fig.14). To investigate the sensitivity of the results presented hitherto to the exact form of the current below 20 cm we have tried a number of forms for the profile, based on both the GMG model generating its own ripple dimensions (Carstens et al., 1969) and also on the model run with ripples defined from Nielsen (1981) for irregular waves alone:

$$\lambda/a = \exp\frac{693 - 0.37\ln^8 M}{1000 - 0.75\ln^7 M}$$

$$\eta/a = 21\,M^{-1.85}$$

where a is the wave semi-excursion and M is a mobility number defined as

$$M = (a\omega)^2/(s-1)gD$$

TABLE 3

Variation in the gross and net vertically integrated sand flux due to the waves during run 302.2 (values in parentheses are ranges). Three 240 s long segments, their wave-induced current speed and period are shown together with values for the complete run

Time period (s)	Wave current (cm/s)			On–offshore flux (mg/cm/s)	
	Onshore	Offshore	Period	Gross	Net
0–240	30	33	5.2	170 (19)	23 (25)
241–480	44	40	6.0	503 (47)	48 (49)
481–720	51	46	6.7	650 (84)	91 (89)
0–720	43	40	5.8	442 (49)	52 (55)

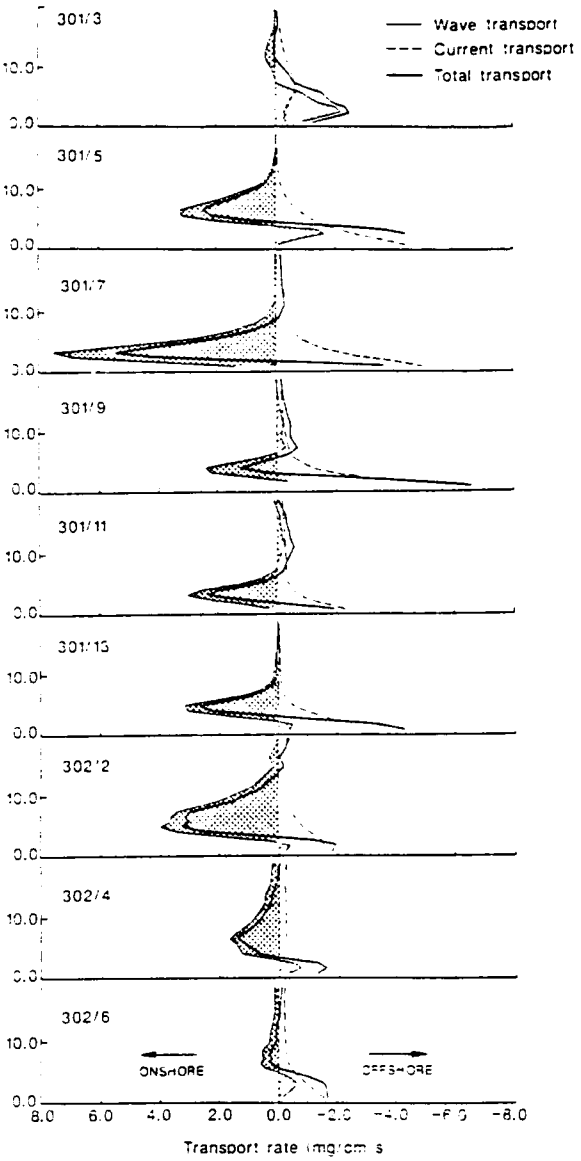

Fig.13. Run-averaged suspended sand transport profiles for the lowest 20 cm (every other run) showing the components due to the steady current and to waves. The cross-hatched region is the shoreward transport due to waves while the diagonal hatching is the offshore transport.

where ω is the wave radian frequency. The transport calculations have been repeated for the four time series shown in Fig.5 using a variety of flow profiles and the results are shown in Table 4 for the crosshore component of the transport. Firstly, the GMG model was run with:

(1) self-adjusting bed topography (Carstens et al., 1969).

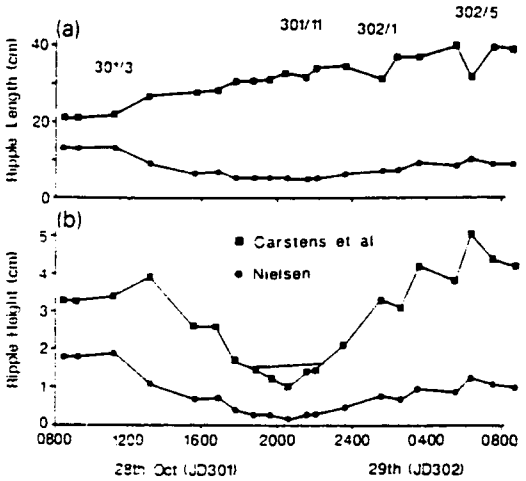

Fig.14. Comparison of the ripple height and length used by the GMG model for combined flow (based on Carstens et al., 1969), and those predicted by Nielsen (1981) for naturally occurring ripples under waves alone.

TABLE 4

The sensitivity of the vertically integrated burst-averaged transport computations to the assumptions about the form of the current profile. The variants (1) and (2) and (a) to (e) are defined in the text. Transport values are in mg cm s. For (c) to (e), shoreward transport is positive

		Q_{mean}		Q_{wave}		
		(a)	(b)	(c)	(d)	(e)
301/3	(1)	8.5	20.5	−8.2	−5.8	−11.0
	(2)	9.5	21.6	−9.7	−7.1	−11.0
301/11	(1)	13.0	20.5	13.2	5.2	15.5
	(2)	10.9	17.9	13.7	5.8	15.5
302/1	(1)	16.6	43.9	24.2	17.6	28.0
	(2)	22.1	52.1	26.7	17.6	28.0
302/5	(1)	3.5	9.3	−5.3	−3.0	−10.8
	(2)	4.7	11.1	−9.8	−4.7	−10.8

(2) GMG model with ripple dimensions from Nielsen (1981) using wave orbital data only (no currents) and then transport calculations made for the steady current Q_{mean} using

(a) the two-layer GMG flow profile, and

(b) a one-layer logarithmic profile defined by the measured current at 20 cm and K_b by the ripple height η.

The wave-induced transport Q_{wave} depends on the profile in the wave boundary layer. The following variants were used:

(c) current profile defined as in eqn.(11),

(d) wave-induced current decreases linearly from the top of the wave boundary layer to zero at the bed, and

(e) wave-induced current constant and equal to the velocity in the potential flow region.

Despite the large differences in the ripple dimensions predicted by the Carstens et al. (1969) laboratory data and Nielsen's (1981) field data, the difference between the transport rates (Table 4 (1) and (2)) is typically only 20%. The transport due the mean current Q_{mean} using the GMG two-layer model gives values which are about half those which are obtained if wave–current interaction is ignored and a simple logarithmic profile assumed (Table 4 (a) and (b)). With the highest sand concentrations occurring close to the bed the form of the wave-induced current profile close to the bed affects Q_{wave} significantly and is sensitive to the form wave profile. The profile (Table 4 (c)) based on the Grant and Madsen (1979) profile (eqn.11) is about mid-way between the results obtained by the linear model (d) and the constant model (e).

7 Discussion

No direct measurements or observations of the dimensions of the bedforms were available for this storm so it was necessary to estimate the amplitude and wavelength indirectly. While this is a severe limitation of the interpretation of the suspended sand data presented here there is sufficient consensus in the literature to suggest that, at wave conditions encountered during this storm, bedform steepness will decrease as wave heights increase.

Following the simple model for vortex shedding (Sleath, 1982) the vortex shed from the crest of a ripple by one wave half-cycle is swept upwards by the next (reversed) half-cycle. As the ripples decrease in steepness, this ejection becomes less efficient and sand is not lifted so high above the bed. At the final stage of an upper phase flat bed, no vortices will be formed and all the turbulence will be generated by the oscillatory flow over the sand grains resulting in a suspension remaining closer to the bed.

7.1 Parameterisation of the reference concentration

Quantitatively the changes in the reference concentration 2 cm above the bed are parameterised through the "constant" γ_0, but this is clearly inadequate for explaining the concentration observations shown in Fig.8. The average skin friction over a rippled bed in the Grant–Madsen–Glenn model is assumed to be equal to that which would occur over a flat bed with the same grain size: the variation in the total drag is assumed to be mainly due to changes in the form drag. These data indicate that there must be considerable variation in the skin friction, averaged over a ripple, compared with a flat bed. They are consistent with a high skin friction over the crests of ripples when the ripples are steep, before the break-off point (Grant and Madsen, 1982) is reached. Beyond break-off point, ripples decrease in steepness and the influence of ripple geometry in enhancing skin friction over the ripple crest decreases (such that the ripple-average skin friction also decreases) and less resuspension occurs.

A best-fit line through the data shown in Fig.10 gives the following relationship between γ_0 and the maximum excess shear stress S_{max} in a wave period:

$$\gamma_0 = 7.5 \times 10^{-3} S_{max}^{-1.8}$$

It is also noted that the values of γ_0 in Fig.10 show a suggestion of hysteresis, the higher values of γ_0 occurring when the waves are increasing in size and hence the ripples would tend to be steeper than their equilibrium value for the waves and sand suspension will be more than expected. As the waves decrease in height the reverse occurs, with ripples being lower and hence less sand would be suspended.

7.2 Transport profiles

Symmetrical waves over symmetrical ripples will result in no net sand transport. The transport profiles computed here, with their maximum wave-induced transport between 4 and 10 cm above the bed, result from flow (and hence bedform) asymmetry. The asymmetry of the wave motion alone is small, the peak currents below the wave crest being only a few centimetres per second faster than below the trough (Table 1); however, from consideration of waves alone the peak shear stress (and hence peak sediment resuspension) would occur beneath the wave crest. At Queensland beach the mean on–offshore current is of the order of 5 cm s^{-1} and is directed offshore (Table 1); this

current and the shear stress associated with it appears be sufficient to bias the peak bed stress towards the offshore wave half-cycle (although the shape of the mean current profile close to the bed is uncertain). With such a stress distribution, the time of maximum resuspension would occur under the wave trough (correlating with the tendency seen in Fig.3 for transport closest to the bed to be offshore) and ripples would have their asymmetry directed offshore. The shoreward flux from 5 to 15 cm is due to the half-cycle following the maximum stress sweeping the suspended sediment cloud upwards into the flow. The sand fall velocity of 2.3 cm s^{-1} and wave period of 5–6 s are consistent with maximum transport at the 5–10 cm height. The importance of the mean current to the direction of the wave-induced transport is also consistent with the transport profiles observed by Vincent and Green (1990) where the mean flow was shoreward and the wave-induced transport pattern was reversed (onshore close to the bed and offshore between 5 and 15 cm).

7.3 *Time and space structure of suspension and bed roughness*

The influence of the groupiness of waves on sediment resuspension has been noted by several authors (Clarke et al., 1982; Vincent et al., 1982) and can be seen in some of the suspension records (Fig.5). The variation in ripple geometry may help to explain this phenomenon. During the passage of a group of waves the sea bed will first be under the influence of small waves (generating steep ripples at equilibrium) and then under larger waves when ripples would be less steep (assuming the break-off point had been exceeded). A time lag would be expected in the response of the bed to the waves, so the big waves in the group would have a bed which was over-steep and which would efficiently eject sand-laden vortices high into the flow and, in the process, erode the ripple steepness. This vortex generation from ripples which are out of equilibrium (over-steep) may allow a series of high waves to advect the decaying vortices high into the water column. Conversely the smaller waves would experience a bed which was flatter than at equilibrium.

Figures 5b and c (301.3 and 301.11) show a good example of this process. From $t = 55$ s to $t = 85$ s in 301.11, virtually no resuspension occurs, yet in 301.3, where the wave-induced current speeds are about the same, resuspension is occurring with every wave and sand is lifted to 20 cm above the bed. We suggest that the difference is due to the more energetic waves prior to $t = 55$ s in 301.11 which have produced ripples of low steepness (approximately in equilibrium with the higher waves). In the low wave period which follows, no vortices can be ejected because of the low steepness and the ripples then start to build in steepness (initially as rolling grain ripples). When the next group of large waves arrives the ripples are over-steep once again and rapid vortex ejection and ripple erosion occurs.

8 Conclusions

Highlighted by these results is the importance of knowing the bed ripple dimensions during suspension events. Unfortunately, photographic techniques for ripple measurement, both video and stills, are very susceptible to any decrease in water clarity and a tracking high-frequency acoustic device is probably the best method for gaining suitable data during sand suspension events (Dingler and Clifton, 1984). Rapid profiling of the bed in the vicinity of the acoustic sand suspension measurements with a vertical resolution of a few millimetres would enable many points of speculation to be resolved, particularly those surrounding the variation in η_0.

The major control on sand resuspension during groupy waves appears to be that of bed topography (ripple steepness) being out of equilibrium with the waves for most of the time, adding a further complication to the problem of modeling suspended sand transport. This also raises the question of the speed at which ripples respond to changing wave conditions: the groupiness of suspended transport suggests a time scale of a few wave periods but if the η_0 values truly show hysteresis the time scale would be very much longer.

Whereas due to the variations in the distributions of sand sizes with height there must be

considerable uncertainty in the accuracy of translating the acoustic measurements into suspended sand concentrations, the points presented here should not be substantially altered because the assumption of a constant distribution should leave the results internally consistent. The measurement of the size distribution variations on time scales of an individual wave, perhaps through the use of multi-frequency acoustics, and its incorporation into the transport profiles must be considered as the next important step in understanding and predicting sand transport in the sea.

Acknowledgements

We wish to thank the very many members of the Universities of Toronto, Dalhousie, Memorial and East Anglia who took part in the Queensland beach experiment, without whom these data could never have been collected. C-COAST is supported by the National Science and Engineering Research Council of Canada. One of the authors (CEV) was supported by a grant from the Royal Society of London and one (DMH) by the U.S. Office of Naval Research.

References

Businger, J.A., Wyngard, J.C., Izumi, Y. and Bradley, E.F., 1971. Flux profile relationships in the atmospheric surface layer. J. Atmos. Sci., 28: 181–189.

Carstens, M.R., Neilson, R.M. and Altinbilek, H.D., 1969. Bedforms generated in the laboratory under oscillatory flow: analytical and experimental study. U.S. Army Corps Eng., Coastal Eng. Res. Cent., Tech. Mem. 28.

Clarke, T.L., Lesht, B., Young, R.A., Swift, D.J.P. and Freeland, G.L., 1982. Sediment resuspension by surface wave action: an examination of possible mechanisms. Mar. Geol., 49: 43–60.

Dingler, J.R. and Clifton, H.E., 1984. Tidal cycle changes in oscillation ripples on the inner part of an estuarine tidal flat. Mar. Geol., 60: 219–233.

Drake, D.E. and Cacchione, D.A., 1989. Estimates of the suspended sediment reference concentration (C_a) and resuspension coefficient (γ) from near-bed observations on the California shelf. Cont. Shelf Res., 9: 51–64.

Dyer, K.R., 1986. Current velocity profiles over a rippled bed and the threshold of movement of sand. Estuarine Coastal Mar. Sci., 10: 181–199.

Glenn, S.M. and Grant, W.D., 1983. A suspended sediment stratification correction for combined wave and current flows. J. Geophys. Res., 92: 8244–8264.

Grant, W.D. and Madsen, O.S., 1979. Combined wave and current interactions with a rough bottom. J. Geophys. Res., 84: 1797–1808.

Grant, W.D. and Madsen, O.S., 1982. Movable bed roughness in unsteady oscillatory flow. J. Geophys. Res. 87: 469–481.

Hazen, D.G., Huntley, D.A. and Bowen, A.J., 1988. UDATS: a system for measuring nearshore processes. Proc. Oceans '88, pp.993–997.

Hanes, D.M., Vincent, C.E., Huntley, D.A. and Clarke, T.L., 1988. Acoustic measurements of suspended sand concentrations in the C^2S^2 experiment at Stanhope Lane, Prince Edward Island. Mar. Geol., 81: 185–196.

Hill, P.S., Nowell, A.R.M. and Jumars, P.A., 1988. Flume evaluation of the relationship between suspended sediment concentration and excess boundary shear stress. J. Geophys. Res., 93: 12,499–12,509.

Huff, L. and Fiske, D.C., 1980. Development of two sediment transport instrument systems. Proc. ASCE Conf. Coastal Eng., 17th, pp. 245–253.

Libicki, C., Bedford, K.W. and Lynch, J.F., 1989. The interpretation and evaluation of a 3 MHz acoustic backscatter device for measuring benthic boundary layer sediment dynamics. J. Acoust. Soc. Am., 85: 1501–1511.

Nielsen, P., 1981. Dynamics and geometry of wave-generated ripples. J. Geophys. Res., 86: 6467–6472.

Sheng, J. and Hay, A.E., 1988. An examination of the spherical scatterer approximation in aqueous suspensions of sand. J. Acoust. Soc. Am., 83: 598–610.

Sleath, J.F.A., 1982. The suspension of sand by waves. J. Hydraul. Res., 20: 439–452.

Smith, J.D. and McLean, S.R., 1977. Boundary layer adjustments to bottom topography and suspended sediments. In: J.C.J. Nihoul (Editor), Bottom Turbulence. Elsevier, New York, pp.123–152.

Vincent, C.E. and Green, M.O., 1990. Field measurements of the suspended sand concentration profiles and fluxes, and of the resuspension coefficient over a rippled bed. J. Geophys. R., 95: 15,591–15,601.

Vincent, C.E., Young, R.A. and Swift, D.J.P., 1982. On the relationship between bedload and suspended load transport on the inner shelf, Long Island, New York. J. Geophys. Res., 87: 4163–4170.

Vincent, C.E., Hanes, D.M., Tamura, T. and Clarke, T.L., 1986. The acoustic measurement of suspended sand in the surf-zone. Int. Conf. Measuring Techniques of Hydraulics Phenomena in Offshore, Coastal and Inland Waters. Br. Hydraul. Res. Assoc., London, pp.443–451.

Wiberg, P. and Smith, J.D., 1983. A comparison of field data and theoretical models for wave-current interactions at the bed on the continental shelf. Cont. Shelf Res. 2: 147–162.

Accepted for publication, Journal of Geophysical Research –OCEANS, 1991

Suspension of Sand Due to Wave Groups

Daniel M. Hanes

Coastal and Oceanographic Engineering Department

University of Florida

Gainesville, Florida 32611

Abstract

Field observations of the suspension of sand near the sea bed under shoaled waves in the nearshore region are presented and discussed with regard to the influence of wave groups. Sand is found to be suspended at both the incident wave frequency and also at lower frequencies corresponding to wave groups. These limited observations indicate the likelihood that wave groups result in higher concentrations of suspended sand than randomly distributed waves of similar heights.

Introduction

The suspension of sand within approximately 10 cm of the sea bed in nearshore regions has been observed to occur in an event–like manner over a range of time scales (Brenninkmeyer, 1976; Hanes and Huntley, 1986; Sternberg et al., 1989; Hanes, 1990). Although time scales for near bed sand suspension comparable to the period of the surface gravity waves were reported, the same investigators also reported that suspension occurred at longer time scales corresponding to infragravity waves or wave groups. Because sand near the sea bed in still water would sink to the bed in a few seconds, suspension at longer time scales would seem to require fluid motion at the same time scales. In the case of infragravity wave motion there can be highly energetic low frequency fluid motion which could

cause sediment suspension. Observations of this phenomenon were reported by Beach and Sternberg (1987). In contrast, there is no fluid motion at the wave group time scale due to the wave groups alone, so the dynamical links between shoaling wave groupiness and sand suspension are not obvious. One well described and relevant hydrodynamic phenomenon related to wave groups is the forcing of a low frequency wave bound to the wave groups (Longuet–Higgins and Stewart, 1964). Shi and Larson (1984) suggested that the bound long wave in combination with wave groups would result in offshore sediment transport. This result is based on the reasonable assumption that more sand will be suspended during intervals of larger waves, which will be coincident with the offshore phase of the bound long wave. However, no sediment transport models or theories predict a group related time scale for suspension or an enhancement of suspended sediment concentration during grouped sequences of large waves, relative to that which would occur if the same waves were randomly distributed.

The general physical linkages between the fluid forcing and sediment response are not well known under unsteady forcing conditions. If suspended sediment concentration were instantaneously proportional to the near–bed velocity raised to an even power, for example, then the low frequency envelope seen in the velocity record during wave groups would be reflected in the suspended sediment record. This partially explains the field observations to be presented. However, it will be shown through spectral analysis techniques that the suspended sand concentration is actually enhanced during wave groups.

The field measurements to be described were obtained in the nearshore region at Cape Canaveral, Florida with the use of a pressure sensor, a 2-axis electromagnetic flowmeter, and an acoustic concentration meter. The flowmeter was centered approximately 15 cm above the sea bed. The averaging volume of the flowmeter was approximately 1 liter, and the amplitude response was near unity for frequencies below 1 hz. Accuracy in the fluid speed measurements is better than 5 cm/s. The acoustic concentration meter measured the vertical profile of suspended sand concentration. The temporal and spatial resolution

of the concentration measurements were 0.25 seconds and 0.5 cm, respectively. Based upon laboratory calibration, the uncertainty in the concentration measurements are believed to be approximately 10% for the relative concentration, and 25% for the absolute concentration. These uncertainties do not significantly influence the results to be reported here.

The data were obtained over a 6 hour period on the evening of July 13, 1988, in the region just outside the surf zone in water depth of about 2 m. The tide rose about 25 cm during the first 3 hours, and dropped about 50 cm during the last 3 hours. Data consists of time series recorded at a rate of approximately 4 hz for 8.7 minutes each hour, so the duration of data presented is approximately 52 minutes. The significant wave height at the sensors varied about 20% over the duration of these observations. It was approximately 40 cm with a peak wave period of 8 to 9 sec. The mean cross-shore current measured by the flowmeter was 7.1 cm/s, directed offshore. The local sand had a narrow size distribution with mean sieve diameter of 0.18 mm. The sea bed was flat, with occasional shell fragments protruding up to 2 or 3 mm above the sand.

The data will be described below in both the time and frequency domains. Both techniques will be used to demonstrate the correlation between near bed suspended sediment concentration and wave groups. The quantity U^2 is chosen to characterize the wave forcing because of its usefulness in describing the wave groupiness. U^2 is also a measure of the fluid speed, wave height, bottom shear stress magnitude, energy density, etc. The dynamical dominance of any one of these quantities is not implied, and the identification of specific processes causing the correlations to be presented below remains as future work.

A time series of suspended sediment vertically averaged over the region 0.5 cm to 4.5 cm above the sea bed (NBC) is shown in Figure 1 along with U^2, where U is the cross-shore component of the fluid velocity. Figure 1, which shows the first of the six data runs, illustrates the previously mentioned observation that suspension occurs at a time scale near that of the incident waves, and also at longer time scales. The longer time scales are further illustrated in Figure 2, which shows lowpass (30 sec) filtered time series of both U^2 and

NBC for the entire six records, plotted in sequence with a sliding ordinate. The visual correlation at long time scales is striking. Correlations to be presented below are calculated as follows. NBC and U^2 for each data run are lowpass filtered and cross correlated. The maximum correlations are then averaged. The results are presented in tabular form below:

Lowpass Filter	Correlation	95% Confidence Limits
None	.30	.29 to .31
30 second	.71	.59 to .79
100 second	.67	.41 to .83

The confidence limits are estimated assuming normal distributions with 12228, 102, and 31 degrees of freedom. These correlations are remarkably high; they strongly support the hypothesis that wave groupiness is causally linked to nearbed sand suspension.

Figure 3 presents the power spectrum of NBC and U^2 along with the 95% confidence intervals. Individual spectra were computed using 1024 point fft's with no overlap, and then averaged together. In contrast to the spectrum of U (not shown) which has one to two orders of magnitude less variance at the group periods compared to the incident band, the spectra of U^2 and NBC show considerable variance at low frequencies. As alluded to previously, one could argue that the suspended sediment concentration is instantaneously proportional to U^2, and that suspension at group time scales simply reflects U^2 at group time scales. If the NBC were perfectly linearly related to U^2, then the spectral ratio between NBC and U^2 would be constant. Rather, Figure 4 shows that this ratio increases as much as a factor of 2 to 3 in the 50 second to 100 second range of periods.

Figure 5 shows the spectral coherence (computed as before) between U_f^2 and NBC, where U_f is the high pass filtered U with a cutoff of 20 seconds. The purpose of examining U_f^2 is to remove any low frequency fluid motion which may be unrelated to wave groups. The high coherence between U_f^2 and NBC over a broad range of low frequencies clearly demonstrates the effect of wave groupiness, isolated from direct (non–group induced) fluid forcing at low

frequencies. Coherences above the dashed line indicate with 95% confidence that NBC and U_f^2 are not linearly independent.

In conclusion we have identified two features of a set of field observations of near bed sand suspension under shoaled wave, flat bed conditions. Firstly, there is a significant correlation between near bed concentration and cross-shore fluid speed squared over a range of time scales, and secondly, the concentration is enhanced at time scales corresponding to groups of incident waves.

Acknowledgments

The author wishes to acknowledge the support of the Naval Civil Engineering Laboratory and the U.S. Office of Naval Research Coastal Sciences Program, and thank M. R. Erdman for his assistance.

References

Beach, R.A., and R.W. Sternberg, 1987. The influence of infragravity motions on suspended sediment transport in the inner surf zone of a highly dissipative beach, Coastal Sediments '87, A.S.C.E., 913-928.

Brenninkmeyer, B.M., 1976. In situ measurements of rapidly fluctuating, high sediment concentrations. *Marine Geol.*, 20, 117–128.

Hanes, D.M., 1990. The structure of events of intermittent suspension of sand due to shoaling waves. In *The Sea*, Volume 9: Ocean Engineering Science, Chap. 28, B. Le Mehaute and D. M. Hanes, eds., pp. 941–952.

Hanes, D.M. and D.A. Huntley, 1986. Continuous measurements of suspended sand concentration in a wave dominated nearshore environment. *Continental Shelf Research*, 6 (No. 4), 585–596.

Longuet–Higgins, M.S., and R.W. Stewart, 1964. Radiation stress in water waves; a physical discussion, with applications. *Deep–Sea Research*, 11:520–562.

Shi, N.C., and L.H. Larson, 1984. Reverse sediment transport induced by amplitude–modulated waves, *Marine Geology*, 54:181–200.

Sternberg, R.W., N.C. Shi, and J.P. Downing, 1989. Continuous measurements of suspended sediment. In *Nearshore Sediment Transport*, Chap. 11A, R.J. Seymour, ed. Plenum, New York, pp. 231–257.

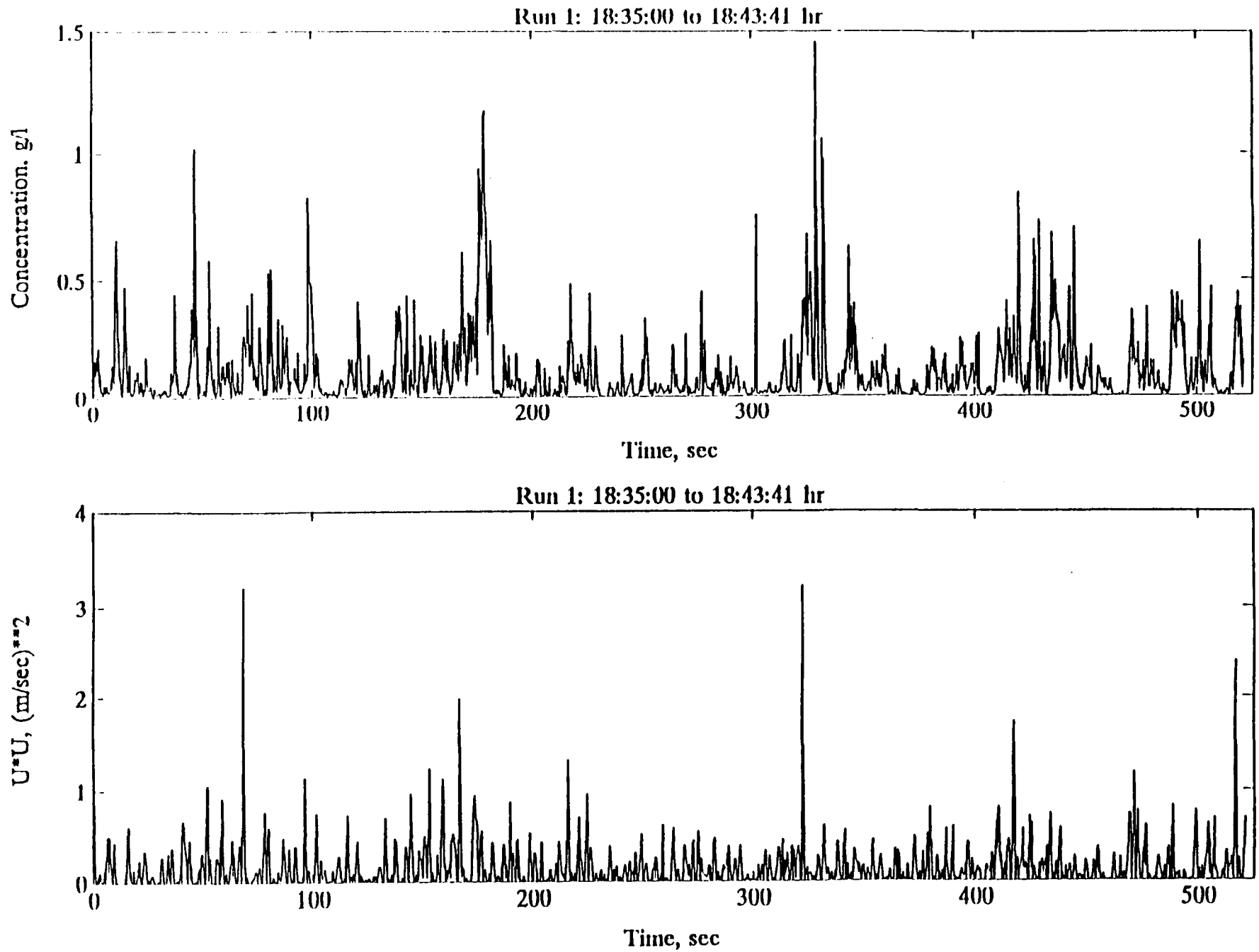

Figure 1: Time series of NBC and U^2 for the first of six data runs.

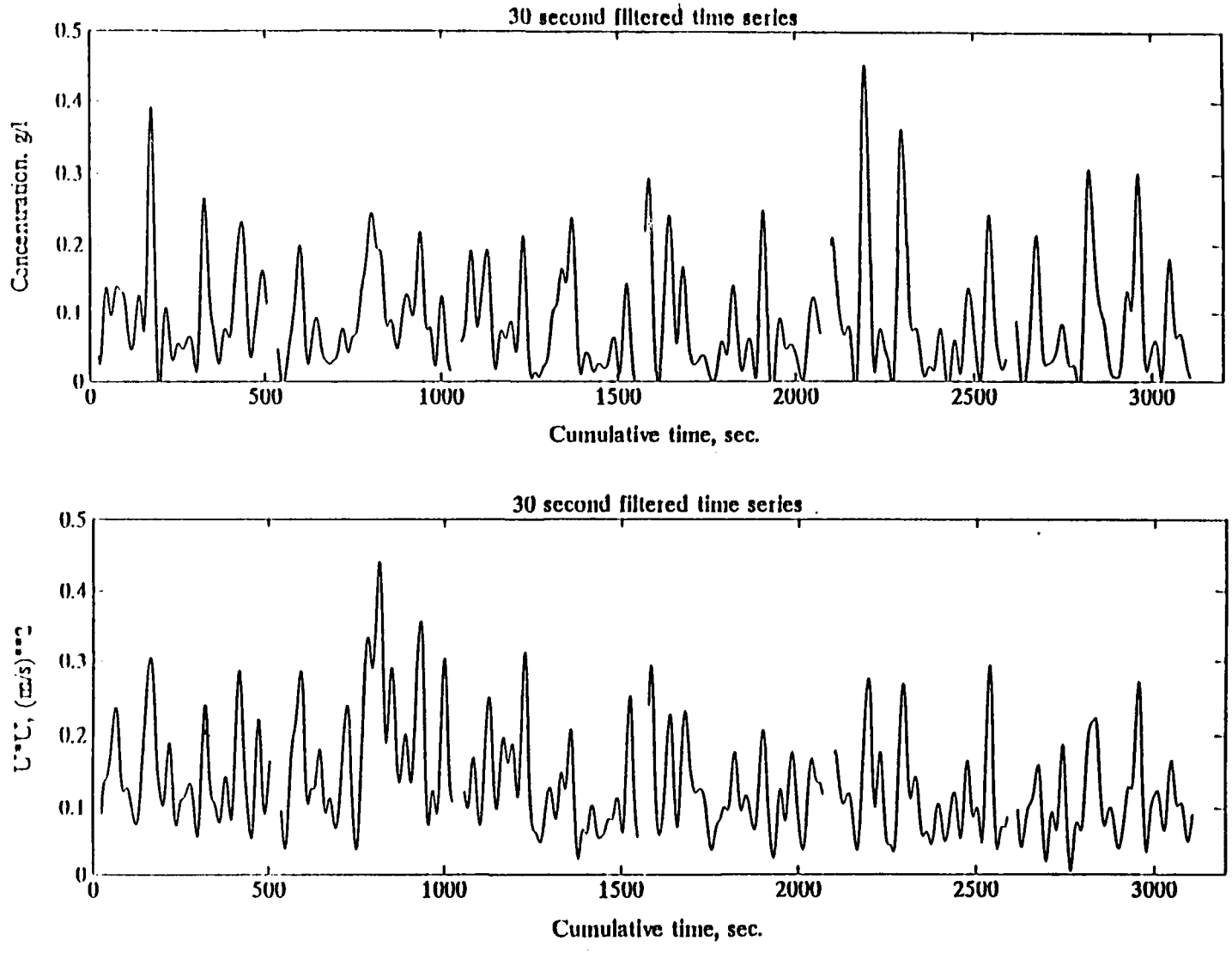

Figure 2: Time series of lowpass filtered (30 seconds) NBC and U^2. The time axis is sliding so that the six data runs are plotted in sequence.

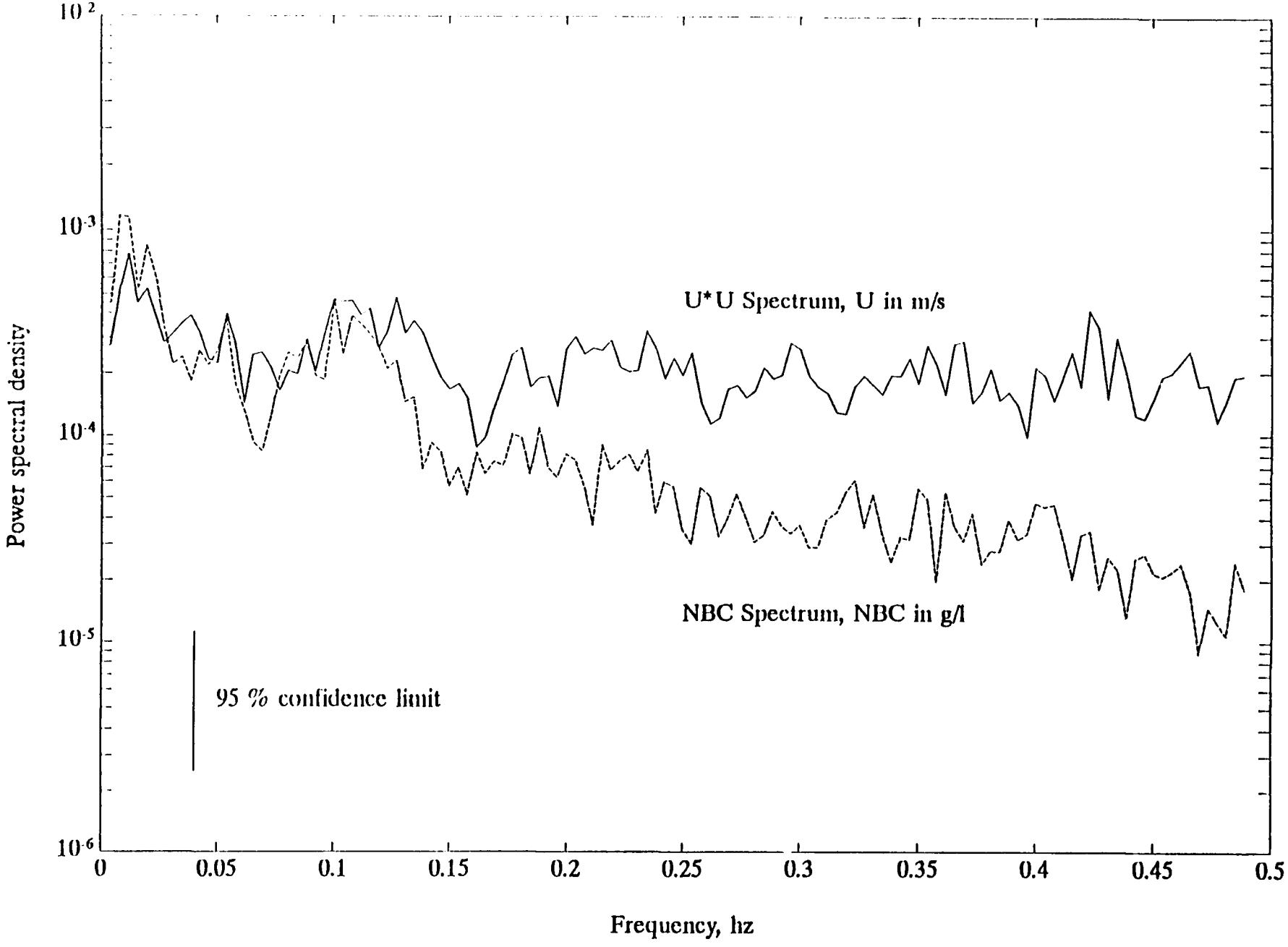

Figure 3: Spectra of NBC and U^2.

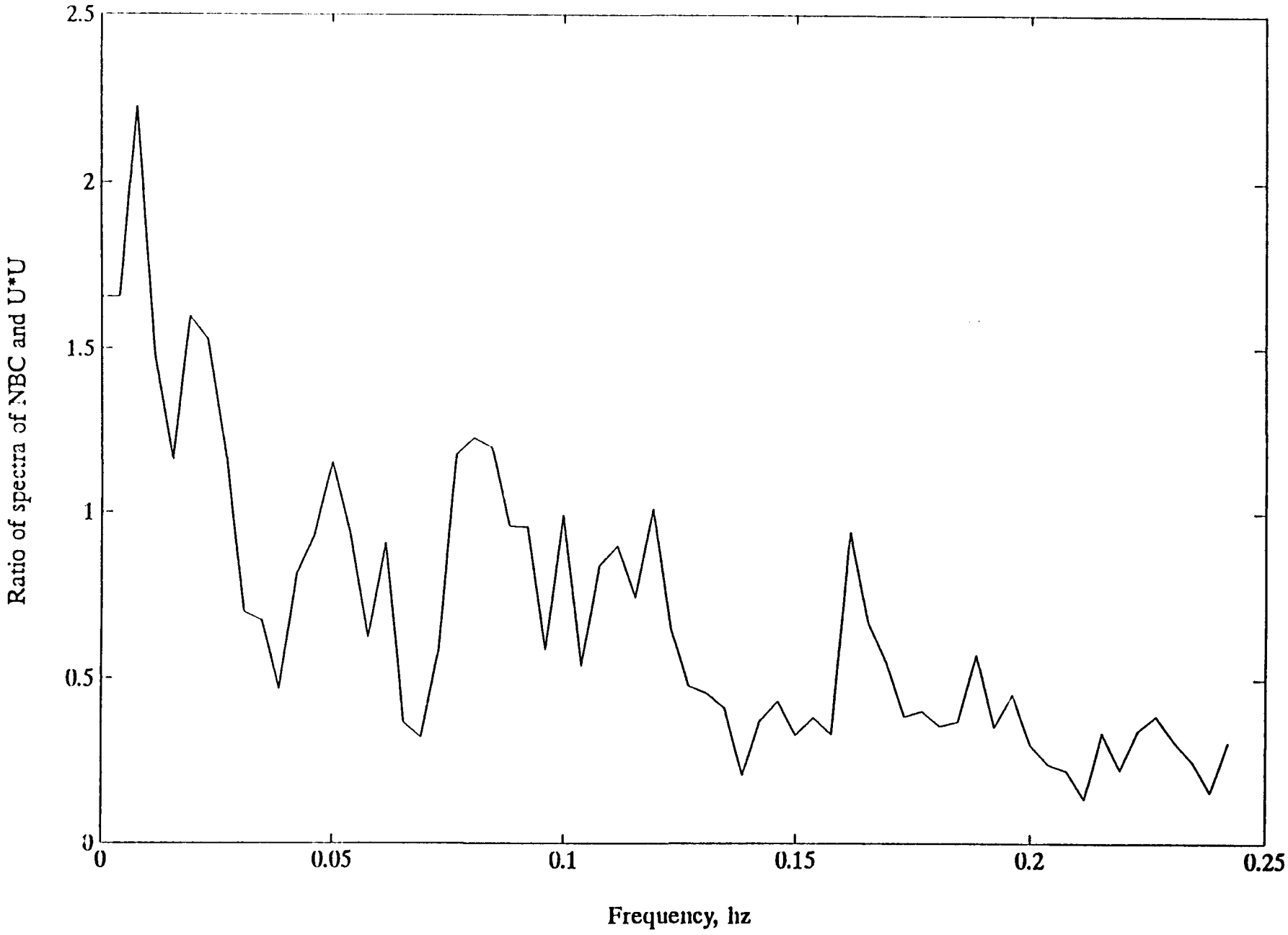

Figure 4: Spectral ratio of NBC to U^2.

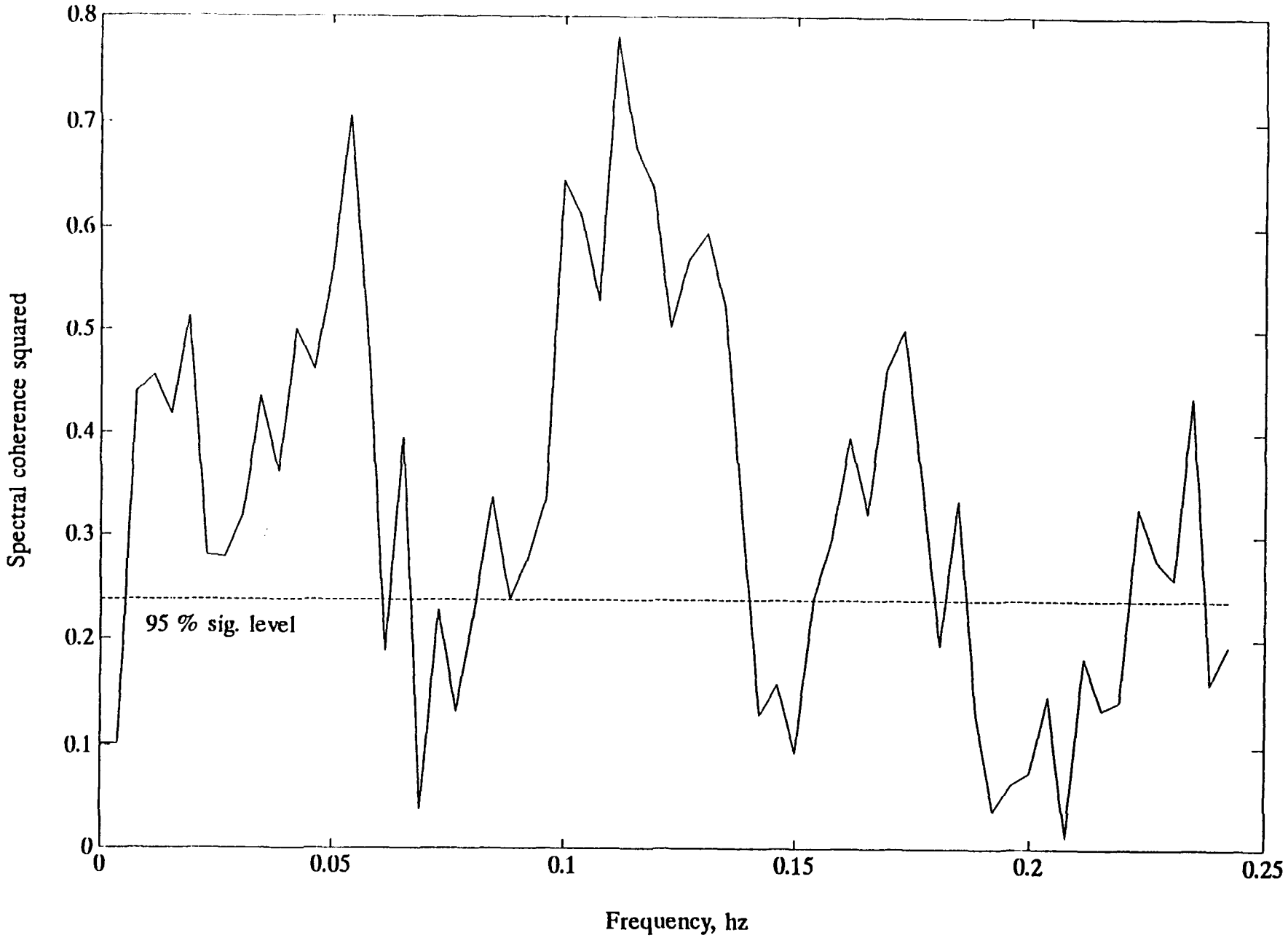

Figure 5: Cross-spectral coherence between U_f^2 and NBC, where U_f is high passed filtered (20 sec) U.